Earth-Science Reviews 196 (2019) 102880

Contents lists available at ScienceDirect

Earth-Science Reviews

journal homepage: www.elsevier.com/locate/earscirev

Mercury as a proxy for volcanic emissions in the geologic record

Stephen E. Grasby[a,*], Theodore R. Them II[b], Zhuoheng Chen[a], Runsheng Yin[c], Omid H. Ardakani[a]

[a] Geological Survey of Canada, Natural Resources Canada, 3303 33rd St NW, Calgary, AB T2L 2A7, Canada
[b] Department of Geology and Environmental Geosciences, College of Charleston, Charleston, SC 29424, United States of America
[c] State Key Laboratory of Ore Deposit Geochemistry, Institute of Geochemistry, Chinese Academy of Sciences, Guiyang 550081, China

ARTICLE INFO

Keywords:
Mercury spikes
Large Igneous Province
Mass extinction
Ocean anoxic event

ABSTRACT

Large igneous province (LIP) eruptions are increasingly considered to have driven mass extinction events throughout the Phanerozoic; however, uncertainties in radiometric age dating of LIP materials, along with difficulty in accurate age dating of sedimentary rocks that record the environmental and biological history of our planet, create inherent uncertainties in any linkage. As such, there is interest in using geochemical proxies to fingerprint periods of major volcanism in the sedimentary record (termed here LIP marks). The use of sedimentary mercury (Hg) contents has been suggested to be the best tool to accomplish this goal, and recent work is reviewed here. Studies to-date show that most extinction events, ocean anoxic events, and other environmental crises through the Phanerozoic have an associated sedimentary Hg anomaly. It remains unclear though if each Hg anomaly is truly a signature of massive volcanism, or if it is controlled by local or regional processes. As Hg has a strong affinity to organic matter (OM), normalisation with total organic carbon (TOC) has been used to assess anomalies. The measurement of TOC has been fraught with error throughout many studies, leaving some claimed Hg/TOC anomalies questionable. Normalisation by other elements that can affect Hg sequestration, such as Al and S, are less common but warrant further investigation. Stable isotope systematics of Hg have helped to further clarify the origin of Hg spikes, and clearly show that not all Hg anomalies are directly related to volcanism. Although a promising tool, the Hg proxy requires more refinement to accurately understand the nuances of an Hg anomaly in the rock record.

1. Introduction

Over the last 250 years, large volcanic eruptions (> 10 km^3 magma) have affected Earth's climate in a similar manner to that of El Niño events, whereby global climate systems were perturbed over several years following eruptions (Robock, 2000). Cooling effects have also been observed in the world's oceans for decades after eruptions (Gleckler et al., 2006). Large eruptions have even induced crop failures and mass starvation at various points in human history (Self, 2005). It stands to reason then, that extremely large eruptions in Earth's history could have had extreme environmental impacts, beyond comparison to those observed in recent history. The largest eruptions in the geologic record (> 100,000 km^3 of magma) are known as large igneous province (LIP) events (Ernst and Youbi, 2017) – eruptions that are four orders of magnitude greater than any known in human history. Growing evidence has shown temporal linkage between LIP events and the largest mass extinctions of the Phanerozoic (Bond and Grasby, 2017; Bond and Wignall, 2014; Courtillot et al., 1999; Courtillot and Renne, 2003; Ernst and Youbi, 2017; Wignall, 2001), suggesting that these sporadic events have shaped evolution of life on the planet. There is an underlying challenge, however, to show a true cause-and-effect relationship between LIPs and extinctions. While the volcanic rocks themselves can be dated with increasingly high-precision radiometric isotope systems, age uncertainties can still be larger than the time frame of extinction events themselves. The sedimentary rocks that record the extinction events are even more difficult to accurately date, especially if zircon-bearing ash beds are lacking. This challenge of linking a LIP to an extinction is well illustrated by the debate over the role of the Deccan Trap LIP event during the end-Cretaceous mass extinction (Burgess, 2019; Schoene et al., 2019; Sprain et al., 2019). Thus, definitive demonstration of a temporal linkage between environmental crises recorded in the sedimentary record, and LIP events that may be driving them, remains elusive. As such, there has been strong interest in the development of chemostratigraphic proxies for volcanic emissions. A proxy that has received much interest in recent years is the use of mercury (Hg) anomalies in sediments as a signature for large volcanic eruptions, as suggested by Sanei et al. (2012).

Volcanoes are a primary source of Hg to the global atmosphere.

* Corresponding author.
E-mail address: steve.grasby@canada.ca (S.E. Grasby).

https://doi.org/10.1016/j.earscirev.2019.102880
Received 4 March 2019; Received in revised form 16 May 2019; Accepted 10 June 2019
Available online 12 June 2019

Estimates of average modern volcanic emission rates vary significantly though, from 75 to 700 Mg/ya (Nriagu and Becker, 2003; Pirrone et al., 2010; Pyle and Mather, 2003; Selin, 2009). Annually, this represents ~10% of global atmospheric emissions (pre-anthropogenic; e.g., Driscoll et al., 2013), including recycling of Hg through various reservoirs back to the atmosphere. Modern volcanic emission rates reflect background conditions that are only exceeded by major eruptions (Pyle and Mather, 2003). For example, the 1991 Mount Pinatubo eruption led to a two-fold increase in atmospheric Hg levels recorded in the Austrian Alps (Ansmann et al., 1997; Slemr and Scheel, 1998). Transient increases in Hg concentrations have also been suggested to record major volcanic eruptions over the last several hundred to thousands of years, in ice core records (Schuster et al., 2002), lacustrine sediments (de Lacerda et al., 2017; Gelety et al., 2007; Ribeiro Guevara et al., 2010; Roos-Barraclough and Shotyk, 2003), and peat bogs (Roos-Barraclough et al., 2002). For LIP events, volcanic Hg emission rates would be significantly higher than any recent major eruption and occur over much longer time intervals. For instance, Grasby et al. (2015) estimated that Hg emissions from the Siberian Traps LIP event (~252 Mya) were as great as 3800 MT (10,000 Mg/a, or a ~14× increase over modern background). Similarly, Percival et al. (2015) estimated a total of 150 MT of Hg was released from the Karoo–Ferrar LIP, that occurred over 300–500 kyr (equivalent to 500–3000 Mg/a). To put this into context, recent industrial Hg emissions to the environment, that are of roughly equal proportion to geogenic sources (representing only a 2× increase), have been the subject of major global concern given the toxicity of Hg and its persistence in the environment (AMAP, 2011). Thus, not only is Hg a potential fingerprint for massive volcanism associated with extinction events, it may also be a contributing factor (Grasby et al., 2015).

There remain, however, potential issues with the use of sedimentary Hg as a signature of volcanism. There are other potential Hg sources that could be released, as well as changes to sequestration pathways that could occur, in association with climatic feedbacks of a LIP event. Some studies have employed stable isotope systems of Hg to distinguish sources of Hg in the geologic record (Gong et al., 2017; Grasby et al., 2017; Huang et al., 2018; Shen et al., 2019; Sial et al., 2016; Them et al., 2019; Thibodeau et al., 2016; Wang et al., 2018; Wang et al., 2019; Yin et al., 2017; Zheng et al., 2018), including those that argue not all Hg spikes in the rock record are directly sourced from volcanogenic outgassing (Grasby et al., 2017; Shen et al., 2019; Them et al., 2019; Wang et al., 2018; Zheng et al., 2018). It is then clear that spikes in sedimentary Hg concentrations cannot be simply equated to a definitive signature of volcanism; less clear is what constitutes an “Hg spike” in the first place (i.e., what is the normal background Hg and what exceeds this).

The rapid increase of interest in Hg in the geologic record has produced a tremendous amount of data over the last decade. This provides an opportunity to review published data as a whole, and to assess the usefulness of Hg as a chemostratigraphic tool and proxy for volcanism, as well as some of the associated pitfalls, which we attempt here.

2. Hg in the modern environment

In the natural environment, the dominant phase of mercury emitted from volcanoes is gaseous Hg^0 with an atmospheric residence time of 0.5–1 year, but oxidized (HgII) and particulate Hg (HgP) phases are also released and have residence times on the order of weeks (Bagnato et al., 2007; Driscoll et al., 2013; Hinkley et al., 1999; Lin and Pehkonen, 1999; Pyle and Mather, 2003; Schroeder and Munthe, 1998; Selin, 2009; Witt et al., 2008). This volcanic-sourced Hg is recycled through numerous surface reservoirs such that the dominant source to the atmosphere, on an annual basis, is evasion from the upper ocean and from plants/soil/snow. The phases of mercury with short atmospheric residence times tend to be deposited proximally to emission sources. In contrast, Hg^0 has a long residence time relative to atmospheric mixing, allowing for efficient global cross-hemispheric distribution. Large volcanic eruptions can also generate plumes over 20–40 km high, and thus can inject ash and aerosols into high-velocity stratospheric winds (Thordarson et al., 2009), making global distribution of gaseous Hg and even ash-bound Hg possible (Schuster et al., 2002). For example, observations of the 1883 Krakatau eruption showed that the resulting aerosol cloud injected into the stratosphere circled the globe in 2 weeks (Symons, 1888), and the 1982 El Chichón as well as 1991 Pinatubo aerosol clouds circled the globe in 3 weeks (Bluth et al., 1992; Robock and Matson, 1983).

Volcanogenic Hg is deposited through oxidation of the dominant gaseous form (Hg^0) to reactive Hg^{2+}, which is soluble in water and can be deposited onto land/water through [wet and dry] precipitation. The less dominant particulate forms of Hg, with shorter residence time, are more likely to fall out with ash rapidly. On land, Hg may be deposited onto soil or taken up directly by plant foliage, with Hg concentration of plant tissue increasing as a function of air concentration (Ericksen et al., 2003; Fleck et al., 1999; Frescholtz et al., 2003). Mercury is transferred to oceans through either direct atmospheric deposition (~70%) or riverine transport of Hg bound to terrestrial materials (~30%) such as organic matter (OM) or soil/sedimentary particles (Amos et al., 2014; Holmes et al., 2010). The majority of Hg transported with suspended riverine particles is deposited in ocean margin sediments, with only ~28% reaching the open ocean (Amos et al., 2014). Mercury is also emitted directly to the ocean through subaqueous volcanism and mid-ocean ridge activity (Bagnato et al., 2017; Bowman et al., 2015; Lamborg et al., 2006). In the case of submarine LIP events, Hg distribution may be more limited, due to slower ocean mixing times (e.g. Percival et al., 2018; Scaife et al., 2017).

The Hg cycle (Fig. 1) ultimately ends in long-term (geologic) sequestration in marine sediment, thought to be typically by adsorption of Hg onto OM that settles out of the water column (Fitzgerald and Lamborg, 2014). Amos et al. (2014) suggest in the modern that the dominant long-term Hg sink is in ocean-margin sediments, consistent with these settings also having the highest rates of OM burial. The same authors also suggest that a large and rapid Hg flux to the atmosphere would be cycled through the atmosphere, terrestrial environments, and ocean waters, to be largely sequestered by OM to marine sediments over timescales of centuries, and completely within several millennia. The Amos et al. (2014) modeling results support the hypothesis that Hg released during a LIP event could ultimately lead to an Hg spike in the sedimentary record. Modern studies of anthropogenic Hg release also support that sediments can faithfully record transient (multi decadal) increased Hg flux to the environment in both oxic and anoxic settings, but not always (Gobeil and Cossa, 1993; Goodsite et al., 2013; Lockhart et al., 2000). Studies of modern systems have also shown that Hg is quite immobile and exhibits stable sediment profiles once deposited (Feyte et al., 2012; Outridge and Wang, 2015; Percival and Outridge, 2013) over at least the decadal times scales possible to study, and excepting some marine settings with extremely low sedimentation rates (Gobeil et al., 1999).

Beyond volcanoes, there are other potential mechanisms to create Hg spikes in sedimentary records. These include wood combustion during massive wildfires (e.g., as suggested to have occurred during the Latest Permian Extinction (Shen et al., 2011)) that may create terrestrially sourced Hg spikes localised in nearshore marine environments (Grasby et al., 2017; Them et al., 2019; Wang et al., 2018). Such spikes are consistent with models for increased fire frequency related to climate warming that suggest global Hg flux from forest fires could be > 600 Mg/a (Kumar et al., 2018). These Hg fluxes, however, are within the range of background volcanic emissions, far less than Hg fluxes thought to be associated with a LIP event. If magma intruded into sedimentary basins and induced combustion of coal and other organics (e.g. Grasby et al., 2011; Ogden and Sleep, 2012; Reichow et al., 2009; Saunders and Reichow, 2009), then this could also provide additional

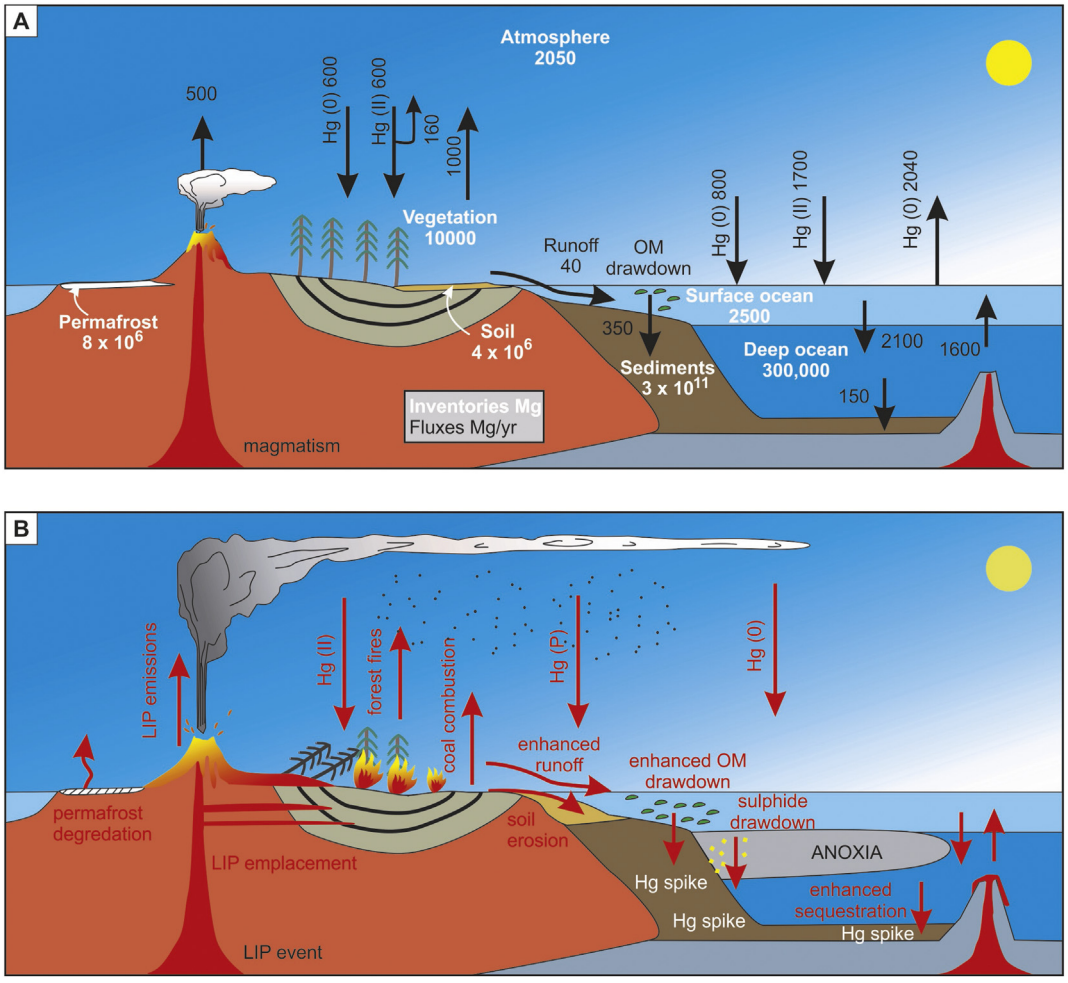

Fig. 1. (A) Schematic diagram illustrating Hg cycle under normal coditions, including estimates of inventories (white text) and fluxes (black text) between reservoirs, after Schuster et al. (2018) and Selin (2009). (B) Illustration of disruptions to the normal global Hg cycle under influence of a LIP event (red text). (For interpretation of the references to colour in this figure legend, the reader is referred to the web version of this article.)

sources of Hg to the environment. Although, like wildfires, the Hg flux from coal combustion would be orders of magnitude less than the Hg associated with volcanic emissions themselves (Sanei et al., 2012). Furthermore, some studies have suggested little volatile materials are released to the atmosphere during the subsurface intrusion of igneous rocks into coals (e.g. Gröcke et al., 2009; Yoksoulian et al., 2016). Permafrost has also been shown to store significant amounts of Hg (Schuster et al., 2018) that could be destabilised during global warming related to LIP-associated CO_2 emissions, potentially providing another significant source of Hg to the environment. Permafrost melting, however, is a self-limiting endothermic reaction, such that melt and release of Hg would occur over several hundred ka (Majorowicz et al., 2014; Majorowicz et al., 2012a; Majorowicz et al., 2012b). As such, permafrost melting should not represent a significant increase in Hg loading rates on short timescales, but rather may lead to an increased Hg flux over 10–100 s of ka. Additional increased Hg fluxes, as indirect consequences of a LIP event, could also include continental denudation of soil cover (Sephton et al., 2005; Them et al., 2017), or those related to changes in glacial cover (de Lacerda et al., 2017). For all these alternative Hg sources, once released they would move through the Hg cycle in similar ways that result in long-term marine sequestration. Key here then are the three main mechanisms that can contribute Hg to marine reservoirs: 1) dispersed atmospheric deposition (Sanei et al., 2012), 2) focused terrestrial influx from river systems that may locally overwhelm any signature of atmospheric-sourced Hg in nearshore areas (Grasby et al., 2017; Them et al., 2019; Wang et al., 2018), and 3) Hg released from submarine volcanics that would have limited mixing (Percival et al., 2018). The rock record appears to support such multiple Hg sources as distal marine sediments appear dominated by atmospheric deposition of Hg, which is a function of increased loading rates of Hg to the atmosphere; whereas nearshore sediments appear to be dominated by Hg released from the disruption of terrestrial environments (i.e., weathering, wildfires, and erosion (e.g., Grasby et al., 2017; Them et al., 2019)).

3. Hg in the geologic record

The study by Hildebrand and Boynton (1989) was one of the earliest examinations of Hg across an extinction event, whereby they report an Hg anomaly at the KPg boundary and suggest potential association with increased acid rain and leaching of metals related to a bolide impact. Similarly, an Hg anomaly was also observed at the KPg boundary by (Palinkaš et al., 1996). Nascimento-Silva et al. (2011) further studied the Hg record at the KPg boundary and suggested that, rather than a signature of bolide impact, it could instead be associated with volcanic emissions of the Deccan Traps. The paper of Sanei et al. (2012) examined Hg anomalies at the Latest Permian Extinction event (LPE), the most severe mass extinction in Earth history. They demonstrated a significant spike in both absolute mercury concentrations and the ratio of mercury to total organic carbon content (Hg/TOC) associated with the LPE. These authors argued that the observed Hg spike at the LPE was derived from the Siberian Traps LIP, one of the volumetrically

largest volcanic eruptions in Earth history – and thus provided the first direct linkage between the extinction and the putative eruptions. They also suggested that Hg should be used to test evidence for temporal linkage of LIP events associated with other mass extinctions in the rock record. Various research groups have taken up this challenge, having since examined most of the mass extinction boundaries in the Phanerozoic record including the Late Ordovician (Gong et al., 2017; Jones et al., 2017), Frasnian-Famennian (Racki et al., 2018), Capitanian (Grasby et al., 2015; Huang et al., 2018), Late Permian (Grasby et al., 2015; Grasby et al., 2013b; Grasby et al., 2017; Sanei et al., 2012), Smithian-Spathian (Grasby et al., 2015; Grasby et al., 2013b), Late Triassic (Percival et al., 2017; Thibodeau et al., 2016), and End Cretaceous (Font et al., 2016; Keller et al., 2018; Sial et al., 2019; Sial et al., 2016; Sial et al., 2014; Sial et al., 2013), as well as several ocean anoxic events (OAEs) (Charbonnier and Föllmi, 2017; Charbonnier et al., 2017; Fantasia et al., 2018; Percival et al., 2015; Sabatino et al., 2018; Scaife et al., 2017; Them et al., 2019), the end of Snowball Earth conditions (Sial et al., 2010), the Cambrian SPICE event (Pruss et al., 2019), the Hangenberg Event (Paschall et al., 2019), as well as the Palaeocene–Eocene Thermal Maximum (PETM; Jones et al., 2019; Keller et al., 2018). These studies have the remarkable finding that all of the major mass extinction events in the Phanerozoic (the big 5 or big 6 depending on your viewpoint – see Bond and Grasby (2017)) have associated Hg anomalies that have been linked by various authors to LIP activity, as well as several ocean anoxia events and other 2nd order-extinctions and climatic perturbations (Fig. 2, Table 1). In addition, it has been suggested that volcanoes do not all result in negative consequences for life and the environment, whereby the Great Ordovician Biodiversification Event (GOBE), which is also marked by an Hg anomaly, is suggested to have been driven by enhanced volcanic loading of bioessential nutrients into marine systems (Liu et al., 2019).

4. Mercury anomalies

Since 2012, over 4500 Hg analyses in the rock record have been published across various major extinction boundaries in the Phanerozoic record (see Table 1 for reference list). As most studies have focused on anomalous intervals of Earth history when the planet experienced mass extinctions and LIP events, there is a potential data bias as the range of Hg values under background conditions are not as well-studied. This raises the question if observed Hg spikes are truly anomalous, or occur elsewhere in the sedimentary record (i.e. between mass extinctions). Grasby et al. (2016) did demonstrate that constant background Hg levels occur over at least a 12 Ma-long Hg record (from the Late Permian to the Middle Triassic), exceeded only during periods of LIP eruptions. A multi-million-year Hg record reported by Them et al. (2019) also shows background Hg and Hg/TOC values similar in magnitude to the Early Jurassic Toarcian OAE. The reported Hg values from all of these previous studies show a log normal distribution, ranging from lower detection limits for Hg (~ 0.16 μg/Kg) to the highest reported Hg value of 9540 μg/Kg, as shown by the histogram in Fig. 3. Metalliferous black shales have been reported with extremely high Hg values, up to 20,700 μg/Kg (Yin et al., 2017); these shales, however, are thought to represent an unusual environment of hydrogenous metal enrichment and do not reflect Hg sequestration under typical marine conditions. Similarly, Jones et al. (2019) reported Hg values of 90,100 μg/Kg that they suggest may be related to localised hydrothermal vent complexes at the PETM. The extremely high Hg values from these two studies are considered localised outliers and are not considered further in this review.

For published studies, the mean of all reported Hg concentration in sedimentary rocks (dominantly shales) is 62.4 μg/kg, slightly higher than the 50 μg/kg average value for the upper continental crust (Rudnick and Gao, 2014). Previous compilations, based on more limited data, indicate that sedimentary rocks have a range of Hg values 30–50 μg/kg (Fleischer, 1970), which are similar to the mean value

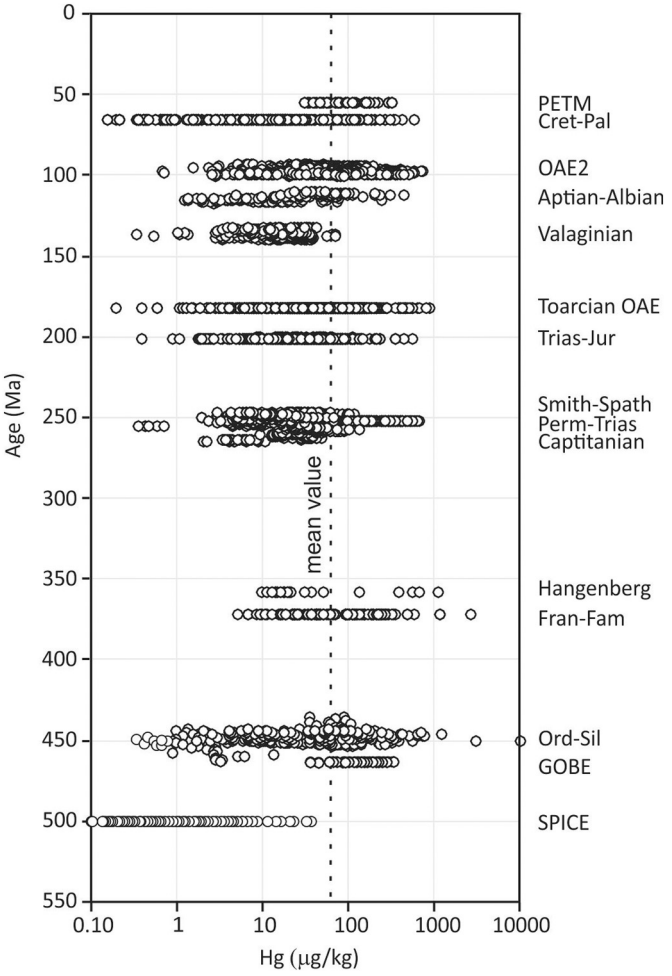

Fig. 2. Reported Hg concentrations at key extinction boundaries and oceanic anoxic events through geologic time. The verticle dashed line represents the mean Hg value of all reproted data. PETM = Palaeocene–Eocene Thermal Maximum, Cret = Cretaceous, Pal = Paleogene, OAE = Ocean Anoxic Event, Trias = Triassic, Jur = Jurassic, Perm = Permian, Fran = Frasnian, Fam = Famennian, Ord = Ordovician, Sil = Silurian, GOBE = Great Ordovician Biodiversification Event, SPICE = Steptoean Positive Carbon Isotope Excursion.

reported here. Approximately half of the reported Hg values have a clear indication of lithology, and of these ~26% are limestone. The mean Hg concentration for limestone is 34.3 μg/kg, suggesting that there may also be lithological controls on Hg concentrations (c.f. Them et al., 2019).

It is instructive to examine Hg spikes, or peak mercury concentrations above local background, for various extinction events as plotted in Fig. 2 and listed in Table 1 relative to the data mean from all studies examined here. Reported "Hg spikes" range from 34.7 μg/kg at the Cambrian SPICE event to 9539 μg/Kg at the Ordovician/Silurian boundary (Gong et al., 2017). At the low end, the Hg spikes fall well below the mean average Hg concentrations and therefore must be questioned as to whether they truly constitute Hg spikes. At the high end, Hg spikes have been suggested to be related to sulphide drawdown, rather than increased Hg loading (Shen et al., 2019), requiring further research to refine. Some extinction boundaries subject to multiple studies also show a range of peak Hg values (Table 1). For instance, studies of Hg spikes at the K/Pg show a high degree of variability, ranging from 46.6 to 576 μg/kg. This variability in peak Hg values may reflect many different processes, such as range of atmospheric transport of Hg from the LIP source, areas of higher primary productivity having greater Hg drawdown, disturbance of local Hg

Table 1
Summary of studies of mercury (Hg) at extinction boundaries and ocean anoxic events (OAEs) through the Phanerozoic showing maximum (peak) reported Hg concentrations and Hg/TOC ratios (TOC = total organic carbon).

Age	Age Ma	Event	LIP event	Peak Hg ppb	Peak Hg/TOC	Max Hg/TOC TOC > 0.2%	Source
Palaeocene-Eocene	55	PETM	North Atlantic Igneous Province	315	1289	1091	Keller et al. (2018)
				90,100	95,676	95,676	Jones et al. (2019)[a]
				262	375	324	Jones et al. (2019)
End Cretaceous	66	KPg	Deccan	257	3131	300	Sial et al. (2016)
				47	960	1.42	Font et al. (2016)
				415	n/a	n/a	Sial et al. (2013)
				576	2590	694	Keller et al. (2018)
Cenomanian-Turonian	93	OAE2	HALIP and others	728	96.5	96.5	Scaife et al. (2017)
Aptian-Albian	120	OAE1b	Southern Kerguelen Plateau	433	3357	1204	Sabatino et al. (2018)
Aptian	121	OAE1a	Greater Ontong Java	~20	~175	?	Charbonnier and Föllmi (2017)
Valanginian	132	Weissert Event	Parana-Etendeka	71	1115	201	Charbonnier et al. (2017)
Upper Jurassic	183	Toarcian OAE	Karoo-Ferrar	838	2590	2590	Percival et al. (2015)
				319	174	174	Them et al. (2019)
				61.6	234	145	Fantasia et al. (2018)
Late Triassic	201.3	End Triassic	CAMP	108	588	410	Thibodeau et al. (2016)
				555	8850	741	Percival et al. (2017)
Early Triassic		Late Smithian Event	Siberian Traps?	65	184	184	Grasby et al. (2016)
				116	150	150	Grasby et al. (2013b)
Late Permian	252	LPE	Siberian Traps	641	1893	1893	Grasby et al. (2017)
				134	275	275	Grasby et al. (2016)
				641	1526	1526	Sanei et al. (2012)
				396	926	255	Wang et al. (2018)
				199	442	442	Wang et al. (2019)
Middle Permian	262	Captitanian	Emeishan flood basalts	48	113	113	Grasby et al. (2016)
				26.6	64.1	64.1	Huang et al. (2018)
Devonian-Carboniferous	359	Hangenberg	?	1090	1557	1557	Paschall et al. (2019)
Devonian	376	Frasnian-Famennian	Center Hill	2517	7102	2044	Racki et al. (2018)
Late Ordovician	443.7	Hirnantian	?	406	342.5	342.5	Gong et al. (2017)
	444.7		?	9539	57,785	626	Jones et al. (2017)
Middle Ordovician	460	GOBD	?	338	139	139	Liu et al. (2019)
Cambrian	500	SPICE	?	35	1577	–	Pruss et al. (2019)

The maximum Hg/TOC ratio is also given for only samples with reported TOC > 0.2 wt%, unless TOC data are not available and then it is listed as n/a. For Pruss et al. (2019) all TOC data are < 0.2 wt% so there are no reported results. The large igneous province (LIP) event thought to be associated with the Hg anomaly is also provided, except for those that do not yet have a clear assocaition (marked by '?'). Note for the Aptian there is no raw data published so values are approximated from the figures.

[a] For the Jones et al. (2019) study extraordinarily high Hg values are reported for the Grane section that are interpreted as a local volcanic source. These values are separated from the other PETM sections they report.

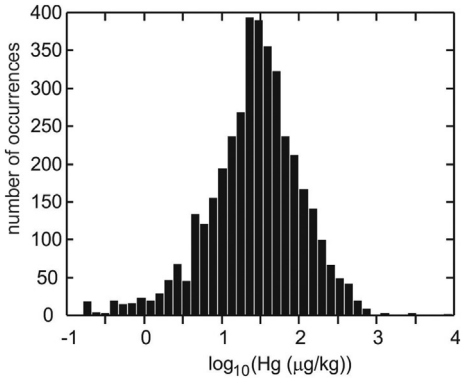

Fig. 3. Histogram showing distribution characteristics of observed mercury values from all previous studies considered here (see Table 1 for references).

reservoirs as a side effect of a LIP event, subareal versus submarine eruptions, or lithologic changes across an extinction boundary (e.g. Percival et al., 2018). Furthermore, as many time intervals studied are associated with local and global redox changes, increased anoxia may play a role in the variability of Hg records through enhanced Hg sequestration (e.g. Sanei et al., 2012; Grasby et al., 2016; Them et al., 2019; Shen et al., 2019).

It is worthwhile to also compare data from the geologic record with Hg data from Pleistocene sediments from the Mediterranean Sea, where Gehrke et al. (2009) show Hg contents of the same order of magnitude (50.9–488 µg/kg) as many ancient sedimentary Hg enrichments linked to massive volcanism. The Hg enrichments in the Mediterranean are suggested by Gehrke et al. (2009) to be all driven by local redox changes and enhanced primary productivity. While one of their Hg spikes does not survive normalisation by TOC, the larger one remains. It remains unclear though if these anomalies are truly related to local redox change, or perhaps provide an Hg record of local volcanism in the Mediterranean (there are 58 recorded volcanic events in the Mediterranean during the Pleistocene (Global Volcanism Program, 2013)). In either case, the Mediterranean record demonstrates that large localised Hg anomalies are possible and are potentially non-unique in the geological record. In general, the data analysis we show here indicates that Hg abundance alone needs to be carefully examined relative to average values in sedimentary rock, and ideally from several locations, to assess if they truly represent anomalous values to warrant the term “mercury spike”.

5. Mercury normalisation

A key challenge in study of Hg anomalies is to assess if increased Hg concentrations are simply related to increased sequestration, rather than increased Hg loading (Sanei et al., 2012). Changes in local bioproductivity, and/or OM flux to a water body, may strongly influence rates of Hg extraction, and consequently Hg concentrations in the underlying sediments. This is observed in modern sediments as a strong

linear correlation between Hg and total OM (Benoit et al., 2001; Gehrke et al., 2009; Outridge et al., 2007; Sanei et al., 2014; Stern et al., 2009), consistent with laboratory studies showing fixed equilibrium constants for Hg binding to OM (Lamborg et al., 2016). Similar observations have been made for the 12 Ma record of (Grasby et al., 2016), suggesting that under background conditions OM is the dominant control on Hg sequestration over geologic time scales. There are other Hg sequestration pathways to also consider. Since they became abundant in the Cretaceous, diatoms may have played a role in Hg sequestration (Zaferani et al., 2018). Mercury can also be extracted from water bodies through adsorption onto clay minerals (Krupp, 1988), leading to a potential relationship between Hg and Al (Sanei et al., 2012; Sial et al., 2016; Sial et al., 2013). While adsorption of Hg onto OM is thought to limit the formation of insoluble Hg sulfide complexes under normal marine conditions (Lindberg et al., 1975; Ravichandran, 2004), Hg-sulphides can form in anoxic environments (Bower et al., 2008; Han et al., 2014). Euxinic conditions could cause local Hg drawdown due to increased localised pyrite burial (Benoit et al., 2001; Sanei et al., 2012; Shen et al., 2019; Them et al., 2019). As well, under oxic conditions Hg can be bound by Fe-oxides in addition to OM (e.g. Kim et al., 2004; Mangold et al., 2014). As such, it becomes critical to examine records of Hg spikes in context of normalised values to OM (as total organic carbon, or TOC), as well as with Al and total sulphur (TS) to help refine our understanding of the principal Hg phases within the sediments, and help to resolve whether Hg anomalies were related to increased atmospheric Hg deposition, or instead other environmental changes in terrestrial and/or marine environments. To date, most studies have restricted analyses to either Hg records alone, or Hg normalised to TOC.

To avoid potential misinterpretation of Hg anomalies associated only with increased OM burial, both absolute Hg concentrations along with Hg normalised to TOC content of the sediment should be examined (Grasby et al., 2013b; Sanei et al., 2012). While this has become fairly standard practice in the literature, not all studies examine both. If only the Hg/TOC value is examined, then a drop in TOC could create an apparent anomaly even if Hg contents did not change. An even larger issue is that when TOC is used to normalise Hg, any measurement error in the denominator (TOC) is magnified in the resultant ratio. Underestimation of TOC will create an artificially high Hg/TOC value. Such potential errors will be magnified as measured TOC levels reach the lower detection limits of the methods used for analyses. Grasby et al. (2013b) suggest that to avoid potential errors related to error in TOC, Hg/TOC values should not be calculated for < 0.2 wt% TOC. Numerous authors, however, have used very low TOC values to assess Hg/TOC anomalies that could lead to spurious results (discussed below). Of the > 4500 reported samples examined here, ~ 84% include TOC analyses, 24% of which are < 0.2 wt% and include extraordinarily low values reported, down to 0.003 wt% TOC (Pruss et al., 2019). Given the use (and abuse) of Hg/TOC values in the recent literature, we review the methods for determining TOC and various errors associated with them prior to examining Hg in the geologic record.

5.1. Total organic carbon (TOC)

Total organic carbon consists of three fractions: (1) extractable OM; (2) pyrolysable carbon (PC); and (3) residual carbon (RC). The extractable OM is composed of the carbon contained in generated hydrocarbon (free oil and gas) in the rock. This fraction is generally a small fraction of TOC. The PC and RC are both part of kerogen and represent labile and inert fractions of OM, respectively (Jarvie, 1991). There are several analytical methods to determine TOC in sedimentary rocks. Among them, loss on ignition (LOI), LECO Carbon Analyzer, and open-system programmed pyrolysis (Rock-Eval and HAWK TOC analyzer) are the most commonly used in geological studies. LOI and LECO methods are based on OM combustion and provide just the TOC content, while pyrolysis methods provide the proportion of the different TOC constituents in the sample (Behar et al., 2001; Lafargue et al., 1998).

Sequential LOI (Dean, 1974; Heiri et al., 2001) is based on weight loss after combustion oxidation of OM. Before combustion, samples are oven-dried and the mass is recorded. OM is then combusted to ash and carbon dioxide, typically between 500 and 550 °C, and then the LOI is calculated based on:

$$LOI_{550} = ((DW_{105} - DW_{550})/DW_{105}) \times 100 \quad (1)$$

where LOI_{550} represent %LOI, DW_{105} represent the sample dry mass before combustion and DW_{550} the dry mass after heating the sample to 550 °C. The mass loss should then be proportional to the amount of organic carbon contained in the sample. Accuracy of LOI measurements can be affected by: (1) incomplete combustion of residual carbon at temperatures < 550 °C; (2) dehydration of clay minerals and metal oxides; (3) decomposition of siderite, magnesite or rhodochrosite at temperatures < 500 °C; and (4) sample exposure time and location in the muffle furnace (Bisutti et al., 2004; Heiri et al., 2001). All of these can lead to overestimation of TOC, particularly at low levels of OM in rocks.

For LECO analyses, samples are first treated with hydrochloric (HCl) or phosphoric acid to remove any carbonates. The rinsed and dried sample is then combusted in an oxygen atmosphere at ~1100 °C, generating CO_2 from conversion of carbon that is measured by an infrared (IR) cell. The mass is converted to percent carbon using sample dry weight. The acid treatment step in this analysis can be a source of error as part of the OM can be hydrolyzed and released to the aqueous phase, as well as floating OM washed out through decarbonation, especially for coal samples (Behar et al., 2001), leading to underestimation of TOC.

Detailed pyrolysis-based TOC analyses are discussed in Lafargue et al. (1998) and Behar et al. (2001). Briefly, a sample is thermally decomposed sequentially in a pyrolysis and oxidation oven to obtain TOC and mineral carbon (MinC), respectively. Hydrocarbons and both carbon dioxide (CO_2) and carbon monoxide (CO) are simultaneously detected via a flame ionization detector (FID for hydrocarbons) and infrared cells (IR cells for CO_2 and CO). In the pyrolysis stage, the sample is introduced into a pyrolysis oven under nitrogen atmosphere and held at 300 °C for 3 min resulting in desorption of free hydrocarbons (referred to as the S1 peak, in mg HC/g Rock). Temperature is then increased at a rate of 25 °C per min up to 650 °C, leading to the thermal cracking of kerogen and subsequent release of hydrocarbons (S2 peak, mg HC/g Rock), organic carbon-sourced CO_2 (S3 peak, mg CO_2/g Rock), and a portion of mineral-sourced carbon (S3′ peak, mg CO_2/g Rock). Following completion of pyrolysis, samples are moved to an oxidation oven where temperature is increased from 300 °C to 850 °C at a rate of 20 °C per min. This phase oxidizes any residual organic carbon (S4CO_2, mg CO_2/g Rock; S4CO, mg CO/g Rock) and the remainder of mineral-sourced carbon (S5, mg CO_2/g Rock). The TOC of the samples is represented as the sum of pyrolysable carbon (PC) and residual carbon (RC).

The comparison of TOC values measured by Rock-Eval 6 and LECO (Behar et al., 2001) showed a significant correlation (R^2 = 0.988) at high TOC, but displayed more scattered data for < 15 wt% samples. This is expected given issues associated with acid treatment in the LECO method (Behar et al., 2001). In general, pyrolysis-based TOC analysis methods are considered to provide the most accurate estimation of TOC in addition to having the benefit of quantifying different fractions of TOC. Caution is needed still where authors do not report the specifics of the pyrolysis instruments, as TOC results are only considered accurate for later model equipment (Rock-Eval6 and HAWK (Carvajal-Ortiz and Gentzis, 2015)).

One inherent problem with use of pyrolysis techniques, however, is that the analytical equipment was developed mainly for the petroleum industry, and as such has a focus on calibration over a range of higher TOC values of interest for petroleum source rock or coal assessment (> 1 wt% TOC). It often becomes difficult to find any clear statement of

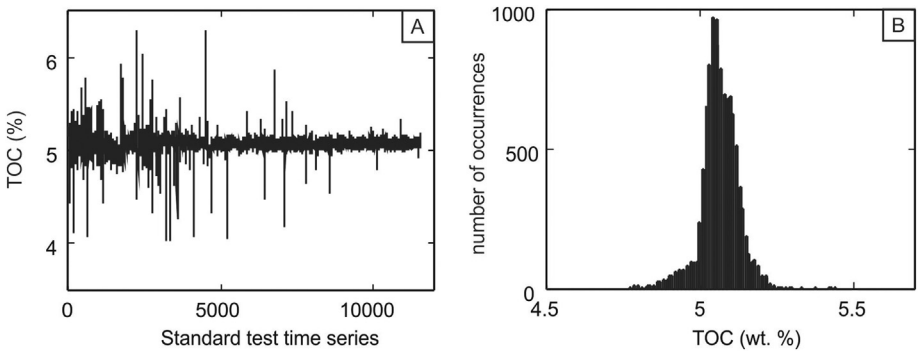

Fig. 4. (A) Time series of measured TOC values. The higher variability early in the record reflects the initial user learning period, and sporadic large deviations through time reflect instrument malfunctions. (B) Histogram of measured TOC values measured as part of standard QA/QC procedures, showing the normal data distribution for 12,542 measurements of the in-house standard.

the lower detection limit of the technique, although 0.2 wt% is a common reported lower limit for pyrolysis. Despite this, instruments (and authors) still report data at much lower values.

To assess accuracy of pyrolysis techniques, we examined the historical records of measured results for TOC standards from the Geological Survey of Canada (GSC). The GSC has routinely measured TOC of an in-house standard for the purpose of QA/QC of the Rock-Eval 6 procedure. A finely powdered (< 212 μm) Cretaceous Second White Speckled shale sample, with a 5.1 wt% TOC content, is analyzed at both the beginning and end of every batch of samples as well as between every 6 and 10 samples within the batch, to ensure the consistency of the data generated over time. From this, > 12,500 analyses over 20 years were accumulated and allows us to derive possible measurement error. Figs. 4A, B are the time series and histogram of these TOC measurements. Large deviations represent obvious equipment errors and are removed from analyses. The mean and two standard deviation of the remaining measurements are 5.06% and 0.164, respectively. Standard deviation is used to express confidence level of the measurement. For a normal distribution, a 95% confidence level covers measurement range from mean plus 2 to mean minus 2 standard deviations, which means that with 95% probability the variation of a measurement can be within a range of 2 standard deviations from the mean in the either side. If a measured value of TOC is close to a 2-standard error, the measured value may not be trustworthy. The 2-standard deviation of TOC from historical measurements of standards is 0.17%, which is consistent with reported 2-standard error of 0.2 for their laboratory source rock standards (55,000 and 64,190) of Behar et al. (2001), supporting the argument of any TOC measurement below 0.2 wt% being unreliable. The robustness of TOC measurements < 0.5 wt% can further complicate Hg/TOC analyses, as an error of 0.17% can result in large relative errors when Hg is normalised to TOC.

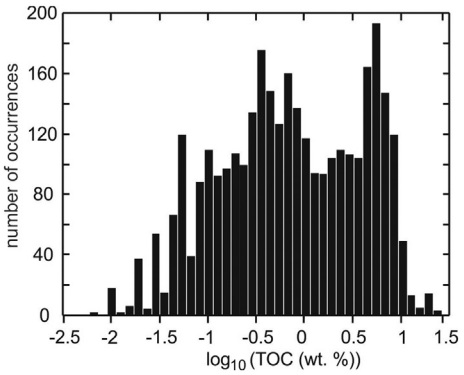

Fig. 5. Histogram showing distribution characteristics of observed TOC values from all previous studies considered here (see Table 1 for references).

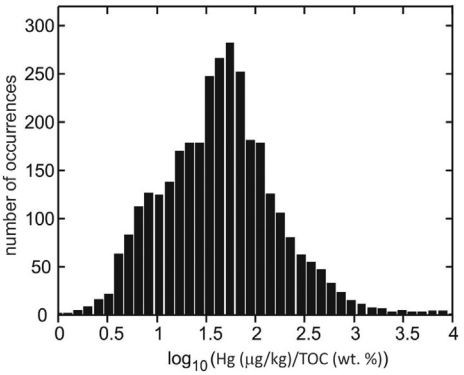

Fig. 6. Histogram showing distribution characteristics of observed Hg/TOC values for all reported TOC values from previous studies considered here (see Table 1 for references).

5.2. TOC normalisation

There are over 3400 TOC values reported as part of Hg studies. These TOC data are plotted in Fig. 5, showing a bimodal lognormal distribution. The reported TOC values range from 0.003 to 26.7% and have a mean value of 2.05%. As discussed, the extremely low TOC values (< 0.2 wt%) are likely unreliable for even the most accurate methods of TOC determination, and caution should be applied when interpreting any records with TOC less than ~0.5 wt%. When examining all published TOC data though, only 2500 TOC values (~75% of the data) are > 0.2 wt%, suggesting that up to 25% of reported Hg/TOC values in the literature are potentially spurious. Furthermore, 44% of the data have TOC < 0.5%, which may also cause spurious Hg/TOC anomalies due to measurements errors. At the other extreme, very high TOC levels represent extraordinarily high OM content of the sediment and are instead probably influenced by local variations in bioproductivity and/or preservation of organic carbon.

To examine Hg/TOC values, we plotted all reported data in Fig. 6. These data show a range from 0.55 to 57,800 μg/kg/wt%, with a mean value of 144 μg/kg/wt%. The same Hg/TOC data are plotted in Fig. 7 as a function of geologic time, showing reported Hg/TOC anomalies relative to the main extinction events as well as OAEs throughout the Phanerozoic. Similar to the Hg concentrations alone, most extinction events and OAEs show large Hg/TOC spikes. That being said, some events, like Cretaceous OAE2, do not have anomalous Hg/TOC values relative to the data mean.

To further illustrate the pitfalls of using spurious TOC values to calculate Hg/TOC, we illustrate the Early Triassic record of the Festningen section. In the study of (Grasby et al., 2016), only Hg/TOC values for TOC > 0.2 wt% were reported and plotted. We show in Fig. 8 these original data along with all Hg/TOC values for samples with TOC < 0.2 wt%. This Figure illustrates that large and spurious Hg/TOC anomalies appear that are driven by TOC values that are below 0.2 wt%. Again, this demonstrates the necessity to avoid using samples with TOC contents below analytical precision of instruments to

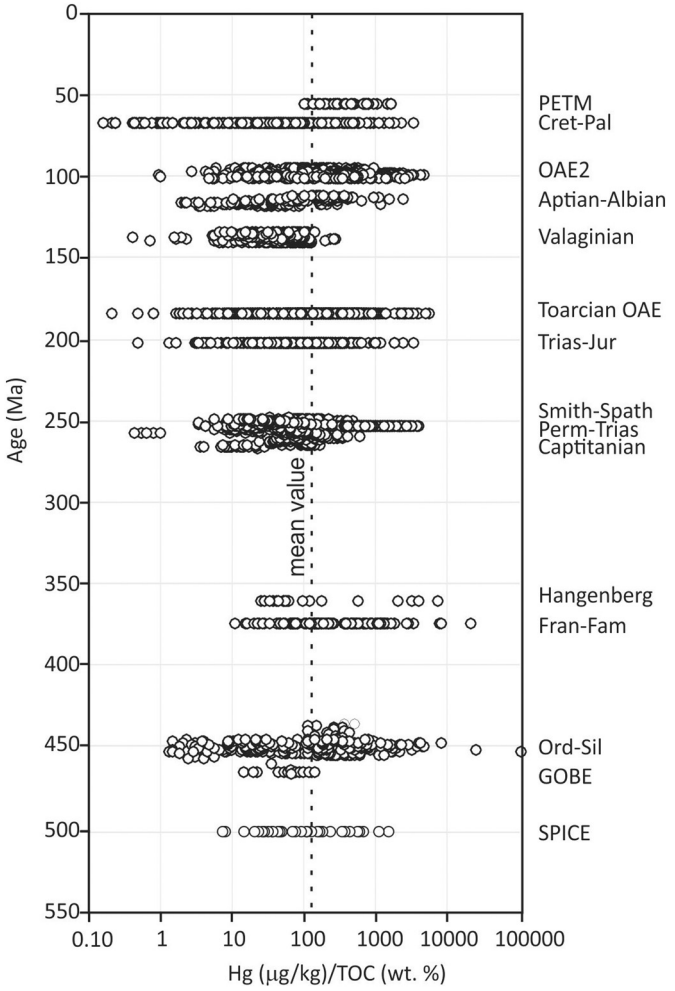

Fig. 7. Plot of Hg/TOC values for all reported TOC values. Vertical dashed line represents the mean value for all data. Abbreviations are defined in Fig. 2.

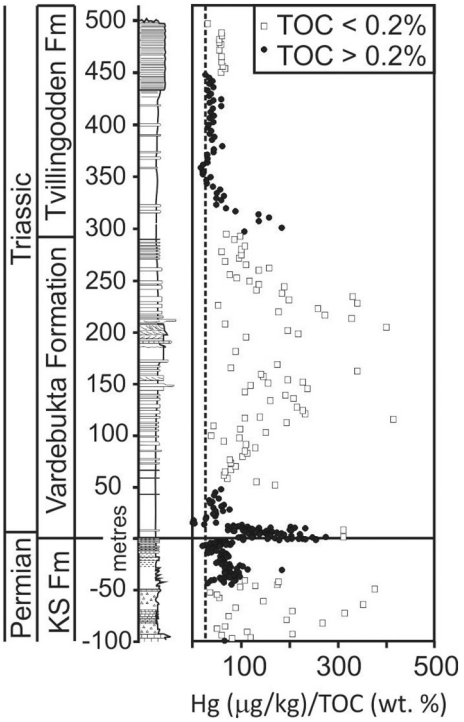

Fig. 8. Plot of data from Grasby et al. (2016) showing difference in results for Hg/TOC values calculated for only TOC > 0.2% (black dots) and with TOC values lower that analytical resolution (white squares). Numerous large Hg/TOC excursions are produced by spuriously high Hg/TOC values created by errors in TOC measurement at low concentrations. The vertical dashed line reflects background Hg/TOC values. The horizontal orange line is the Latest Permian Extinction boundary. Fm = Formation, KS = Kapp Starostin Formation.

calculate Hg/TOC values.

The effect of using inappropriately low TOC values (< 0.2 wt%) to calculate Hg/TOC anomalies can also be observed in a cross plot. Fig. 9A illustrates that the highest reported Hg/TOC values in the literature are restricted to samples with low TOC contents. Fig. 9A also shows that for TOC contents > 2.0 wt%, Hg/TOC values tend to be < 100 (with one exception). These observations suggest that it could be the very low TOC, rather than high Hg, that is responsible for the largest reported Hg/TOC anomalies in the rock record. This can be observed more clearly in Fig. 9B that illustrates only data for TOC values < 2.0 wt%, so as to expand the lower range of the plot shown in Fig. 9A. The data for < 0.2 wt% TOC is shown in the grey box, illustrating that the highest reported Hg/TOC values are restricted to TOC measurements below the lower detection limits of TOC analyses, and thus are most likely spurious and the results cannot therefore be interpreted with any confidence. The mean Hg/TOC value for data > 0.2 wt% TOC is 71.9 µg/kg/wt%, which is ~ 50% of the mean Hg/TOC value for all reported data. If we accept that Hg/TOC values calculated for TOC contents above the 0.2 wt% TOC cut-off as accurate, then the highest reasonable Hg/TOC value reported is 2590 µg/kg/wt%. Fig. 9B also shows that for a portion of the data (those with the highest Hg/TOC values), there is trend of decreasing Hg/TOC with increasing TOC values. Between 1 and 2% TOC, there are no Hg/TOC values > 1000 µg/kg/wt%, and 97% of the data are < 100 µg/kg/wt%. For TOC values < 1%, only 9 samples have Hg/TOC > 1000 µg/kg/wt%, and all of these are associated with TOC < 0.5 wt%. Below 1 wt% TOC, Hg/TOC values > 100 µg/kg/wt% are more common, 398 in total (15% of the data), but even these values tend to be restricted to TOC < 0.5 wt% (88% of samples). It becomes difficult to determine though if this lowering of peak Hg/TOC values with increasing TOC represents an analytical artifact, or instead is reflective of natural processes. For instance, it could be possible the increased Hg loading into environments with lower bioproductivity could obtain, on average, higher Hg/TOC values.

To remove spurious data, Fig. 10 illustrates the same reported Hg/TOC values throughout the Phanerozoic as in Fig. 7, but after samples with TOC < 0.2 wt% are removed. Hg/TOC anomalies are still observed in most studies; for many, however, the maximum Hg/TOC anomaly (after excluding data associated with low TOC values) can be up to an order of magnitude lower than that reported by various authors (Table 1). The SPICE event is removed entirely as all TOC data from that study (Pruss et al., 2019) are well below analytical certainty. This is not to say that a mercury anomaly does not exist in these studies, but instead that the maximum values reported could greatly exaggerate the true scale of the anomaly due to inappropriate use of TOC data. These results require careful consideration of whether it is high Hg, or low TOC, that creates an apparent anomaly in the Hg/TOC value. Based on the mean Hg/TOC value for TOC > 0.2 wt%, we suggest that 71.9 µg/kg/wt% be considered an average value, above which may be considered anomalous.

6. Controls on Hg sequestration

Sanei et al. (2012) discussed potential mechanisms for Hg sequestration over geologic time. They argue that under background marine conditions that OM sequestration is sufficient to mitigate background Hg loading to the oceans. The implication here is that background Hg

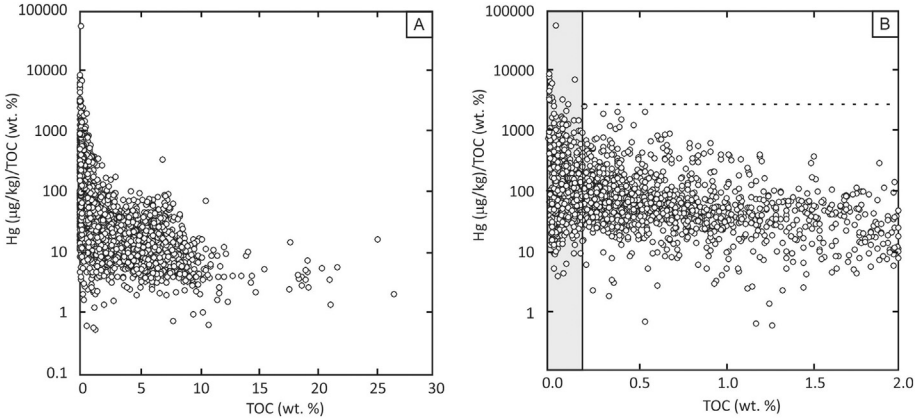

Fig. 9. (A) Plot of all data where TOC is available (~3200 analyses) for Hg/TOC values against reported TOC. (B) Detailed plot of same data as in (A) but showing only data < 2% TOC.

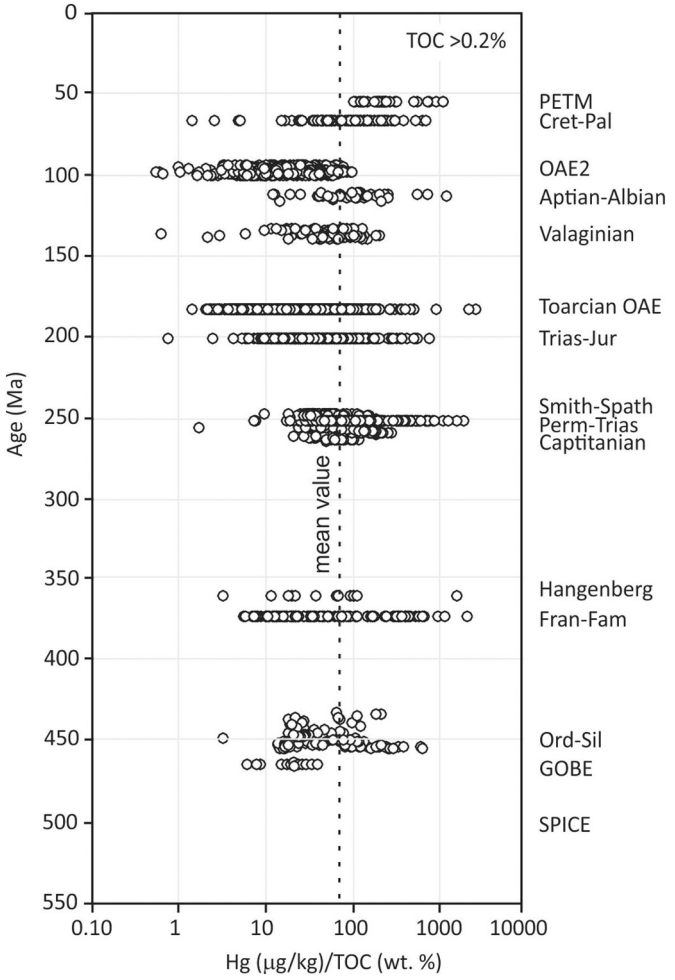

Fig. 10. Plot of Hg/TOC values for samples with TOC > 0.2%. Vertical dashed line represents the mean value for all data with TOC > 0.2%. All data from Pruss et al. (2019) for the SPICE interval are removed as there are no TOC values > 0.2%. Abbreviations are defined in Fig. 2.

emissions are balanced by OM drawdown, preventing any long-term build-up of Hg in the marine reservoir. The study of Grasby et al. (2013b) suggested that OM drawdown of Hg could be defined by a power law relationship:

$$Hg = 48.5TOC^{0.89} \quad (2)$$

implying that the marine Hg pool can even be depleted as primary productivity increased, which is consistent with the results of (Gehrke et al., 2009). Extreme Hg loading associated with a LIP event could overwhelm this normal Hg sequestration system (Sanei et al., 2012) as there appears to be a limit on OM drawdown capacity, as suggested by Lamborg et al. (2016). Without additional mechanism to draw down excess Hg released by LIPs there is potential for development of toxic ocean conditions (Grasby et al., 2015). Development of more expansive oxygen minimum zones as a feedback to LIP CO_2 emissions has been argued to drive the more efficient Hg-sulphide drawdown system (Grasby et al., 2013b; Sanei et al., 2012), mitigating excess Hg in the environment. The large anomalies in Hg concentrations observed at LIP events, with associated peaks in Hg/TOC, are thus thought to reflect increased Hg-sulphide deposition. Whilst most Hg studies do not include sulphur data or paired redox data, we examined the relationship for total sulphur (TS) and Hg in the shale-dominated sequence of the Late Permian through Middle Triassic presented by Grasby et al. (2013a); Grasby et al. (2013b). We show the combined data from these two previous studies in Fig. 11, illustrating that there is no obvious relationship between Hg and TS at low values of TS at these sites. Anomalously high Hg values (greater than the mean average for all data), however, are restricted to TS > 1 wt%.

We analyzed controls on Hg drawdown further by plotting all available Hg and TOC data through the Phanerozoic in Fig. 12A. The logarithmically transformed Hg and TOC concentrations have an overall linear correlation, with a correlation coefficient of 0.63. This relatively strong correlation is again consistent with OM drawdown being a dominant mechanism for Hg sequestration over geologic time.

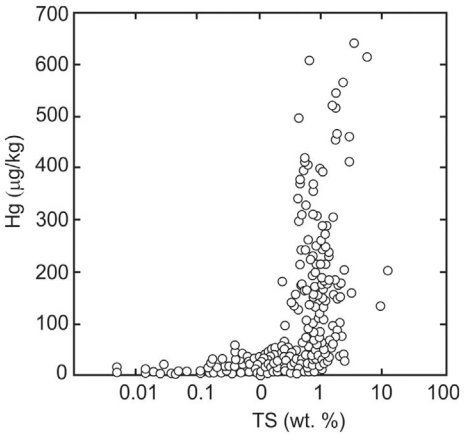

Fig. 11. Plot of Hg vs TS for data from the Sverdrup Basins Late Permian to Early Triassic record.

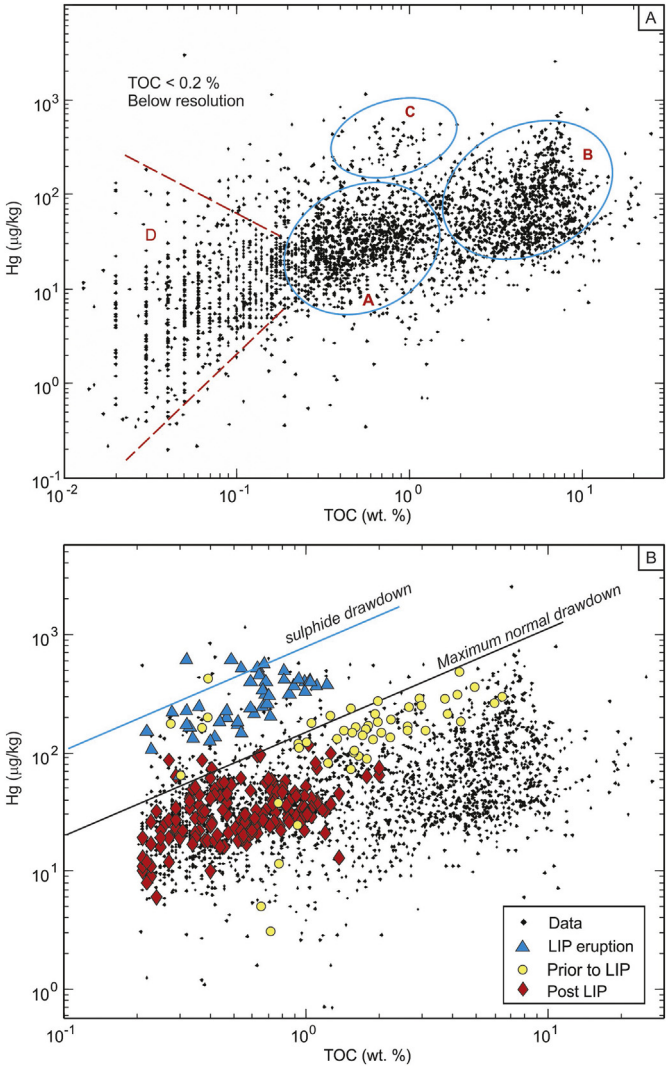

Fig. 12. (A) Cross-plot of Hg and TOC data for all studies considered here, and showing ellipses derived from Grasby et al. (2013b) - labeled A through C, that represent different proposed modes of Hg sequestration. (B) TOC-Hg plot with the dataset from Grasby et al. (2016) superimposed to show variations of TOC and Hg in a relation to records of the largest know LIP event (Siberian Trap eruptions).

The entire dataset in Fig. 12A, in Hg-TOC space, can be compared to the ellipsis derived from Grasby et al. (2013b) labeled A through C), that represent different proposed modes of Hg sequestration. Most data fall within Zone A, and are low in both TOC and Hg, reflecting OM-mediated Hg drawdown under normal marine conditions and background Hg emissions. Data in Zone B are high in TOC (> ~1.5 wt%) and have variable Hg, reflecting high primary productivity environments where OM drawdown begins to limit marine Hg levels. Data in Zone C are low in TOC (0.2 wt% < TOC < 2 wt%) and high in Hg (> 100 mg/kg), reflecting excess Hg drawdown in systems with high rates of pyrite burial. Data points in Zone D (Fig. 12A) are samples with TOC below the 0.2 wt% detection limitation, and are therefore unreliable.

Fig. 12B removes all data points with TOC < 0.2 wt%. Here, based on the remaining data, in additional to the power law function of TOC by Grasby et al. (2013b) in Eq. (2), we propose a similar power law equation to separate the bulk of data in Zones A & B from Zone C, and describe the maximum capacity of mercury sorption by TOC (line of maximum OM drawdown in Fig. 12B). The relationship can be written as:

$$Hg = 150\ TOC^{0.83} \quad (3)$$

Data points in Fig. 12B that fall below the maximum normal drawdown line defined in Eq. (3) would represent settings where Hg concentration is below the maximum sorption capacity of OM. During a LIP event, when Hg loading rates can exceed the capacity of this normal OM drawdown system (zone C of Fig. 12B), a similar power law relationship between the maximum mercury concentration and TOC is proposed to represent the maximum capacity of a joint drawdown by TOC and sulphide (LIP drawdown line of Fig. 12B) as below:

$$Hg = 750\ TOC^{0.83} \quad (4)$$

From the similarity of the two equations, two inferences can be made: a) the two parallel equations may indicate that sulphide and TOC are closely correlated; b) sulphide-Hg drawdown is more efficient way to deplete mercury than TOC in marine setting as indicated by a ratio of two proportionality coefficients 750/150 = 5, meaning that OM sequesters only 1/5 of mercury in Hg spike event. This again points to the importance of normalising Hg data to Al and sulphide to assess other potential drawdown mechanisms. It should also be noted that although TS records are useful for approximating sulphide contents of the sediments and rocks, the sulphurization of OM may lead to an overestimation of sulphide due to these organosulfur compounds (e.g. Raven et al., 2015; Raven et al., 2018). Therefore, pyrite wt% data is ideally required to assess Hg drawdown related to redox changes. For instance, Them et al. (2019) identified a strong correlation between pyrite wt% and total Hg from one section in Germany across the Early Jurassic T-OAE. Shen et al. (2019) have also shown that the Hg in sediments deposited during the Late Ordovician Mass Extinction was hosted by pyrite as a result of local redox variations. These studies again point to the need to separate local redox variations from larger global processes that may form Hg anomalies.

7. Hg isotopes

Mercury has seven natural stable isotopes (^{196}Hg, ^{198}Hg, ^{199}Hg, ^{200}Hg, ^{201}Hg, ^{202}Hg and ^{204}Hg). In the last decade, research into Hg stable isotope geochemistry has provided new insights into the behavior of Hg in the environment (Bergquist and Blum, 2009; Blum et al., 2014; Yin et al., 2014). While investigations of the natural variations of Hg abundances have a longer history dating back to the 1920s (Aston, 1925), it remained challenging until the development of modern techniques using cold-vapor generation multicollector inductively coupled plasma mass spectrometry (CV-MC-ICP-MS) at the beginning of this century (Lauretta et al., 2001). This technique uses a gas-liquid separator, which enables complete separation of Hg from other matrices and continuous introduction of gaseous Hg(0) to the plasma, resulting in low matrix effects, small sample size requirements, and steady signal strength, which are all major challenges for high-precision analysis (Blum and Bergquist, 2007; Foucher and Hintelmann, 2006). Today, mercury isotope compositions are measured exclusively using CV-MC-ICP-MS, with a precision that is at least two orders of magnitude smaller than natural variations (Blum and Johnson, 2017).

Mercury has active redox chemistry, high volatility, and a tendency to form covalent bonds, which provides many opportunities for isotopic fractionation (Bergquist and Blum, 2007). Both mass dependent fractionation (MDF) and mass independent fractionation (MIF) of Hg isotopes are now well documented in experimental studies (Bergquist and Blum, 2009; Blum et al., 2014; Yin et al., 2014). MDF of Hg isotopes is reported using the delta notation, δ, which is the per mil (‰) deviation from a reference material (Bergquist and Blum, 2007):

$$\delta^{xxx}Hg(‰) = (({}^{xxx}Hg/{}^{198}Hg_{sample})/({}^{xxx}Hg/{}^{198}Hg_{standard}) - 1) \times 1000 \quad (5)$$

where ^{xxx}Hg is the isotope of interest. NIST SRM 3133 is the most commonly used reference standard (this is not universally accepted, however). The observation of MIF makes Hg isotope an unusual tracer.

MIF is reported using capital delta notation, Δ, which means the deviation of the measured isotope ratio from the theoretical ratio predicted by MDF:

$$\Delta xxxHg \approx \delta xxxHg - \delta 202Hg \times * \beta \quad (6)$$

where β is an independent isotope-specific constant determined by the theoretical laws of MDF (Bergquist and Blum, 2007).

To date, large variations of Hg isotopic ratios (~10‰ for δ^{202}Hg and Δ^{199}Hg values and ~1‰ for Δ^{200}Hg) have been reported for natural samples (Reviewed by Blum et al., 2014). δ^{202}Hg alone may not be directly used to identify specific sources because MDF is ubiquitous and occurs during all biological reactions (e.g., reduction, methylation, demethylation), abiotic chemical reactions (e.g., chemical reduction, photoreduction, oxidation) and physical processes (e.g., volatilization, evaporation, adsorption, and dissolution) (Bergquist and Blum, 2009; Blum et al., 2014; Yin et al., 2014). The Δ^{199}Hg, Δ^{200}Hg and Δ^{201} values of Hg isotopes also provide unique fingerprints of specific reaction pathways of Hg. Δ^{199}Hg and Δ^{201}Hg anomalies have been predominantly observed on Earth's surface environment in soils, sediments, waters, atmosphere and biological samples, and aqueous Hg photoreactions (e.g., Hg(II) photoreduction and MeHg photodegradation). These Hg photoreactions are thought to play the foremost role in the generation of Δ^{199}Hg and Δ^{201}Hg anomalies in natural samples (Blum et al., 2014; Sonke, 2011; Yin et al., 2016). Aqueous Hg photochemical reactions produces Δ^{199}Hg/Δ^{201}Hg ratios of 1.0–1.3, which is in accordance with the Δ^{199}Hg/Δ^{201}Hg reported in natural samples (Bergquist and Blum, 2007; Yin et al., 2016). Δ^{200}Hg anomalies have been only reported in gaseous elemental Hg (GEM), gaseous oxidized Hg (GOM) species and precipitation (mainly containing GOM), and GEM photo-oxidation seems to be the major cause of MIF for ^{200}Hg (Chen et al., 2012; Gratz et al., 2010; Sun et al., 2016). Overall, combining MDF and MIF, each fractionation process imparts a diagnostic pattern of isotopic variation, and thus Hg isotope ratios can be used to unravel sources and biogeochemical processes of Hg in the environment (Blum et al., 2014).

Over geologic time, Hg is mobilized from deep reservoirs in the earth to the atmosphere through volcanic and hydrothermal activities, and these sources have been shown to have Δ^{199}Hg and Δ^{201}Hg values close to zero (Sherman et al., 2009; Zambardi et al., 2009), although there are not many data from these sources. Aqueous Hg photoreduction (in cloud droplets and surface waters) imparts positive Δ^{199}Hg and Δ^{201}Hg values in residue Hg(II) phase and negative Δ^{199}Hg and Δ^{201}Hg values in Hg^0, largely altering the MIF signals in geochemical reservoirs (Bergquist and Blum, 2007). Precipitation and seawater, which contain Hg(II) species, are characterized by positive Δ^{199}Hg and Δ^{201}Hg values (Chen et al., 2012; Gratz et al., 2010; Štrok et al., 2015). In contrast, terrestrial reservoirs (e.g., plants and soils), which primarily accumulate Hg^0, are generally characterized by negative Δ^{199}Hg and Δ^{201}Hg values, although few positive Δ^{199}Hg values are reported (Biswas et al., 2008; Demers et al., 2013; Enrico et al., 2016; Obrist et al., 2017; Yin et al., 2013; Zhang et al., 2013; Zheng et al., 2016). A summary of reported values from modern environments shows Δ^{199}Hg mean values of gaseous Hg = 0.11‰, wet deposition = 0.39‰, foliage/litter = −0.39‰, and organic soils = −0.25‰ (Sun et al., 2019), supporting the use of Δ^{199}Hg values to distinguish atmospheric versus terrestrial contributions to marine systems. There is some minor overlap with the lowest most range of wet deposition with the highest possible range of terrestrial sources, such that there is room for some non-unique values from −0.2 to 0.1‰ (Sun et al., 2019). Although is difficult to measure the seawater Hg isotopic composition due to extremely low concentrations, coastal seawater Δ^{199}Hg values have a range from ~0 to 0.55‰ (Štrok et al., 2015).

Under normal conditions, natural atmospheric and fluvial Hg emissions appear balanced over geologic time by OM drawdown (Grasby et al., 2013b). Atmospheric deposition represents the major input of Hg to upper open oceans, whereas watershed-derived Hg is predominantly buried in ocean margins (Sunderland and Mason, 2007; Zhang et al., 2015). This is consistent with modern coastal sediments having negative Δ^{199}Hg and Δ^{201}Hg values, which have been explained by watershed input of terrestrially sourced Hg (Yin et al., 2015). In comparison, modern open ocean sediments have positive Δ^{199}Hg and Δ^{201}Hg values, consistent with direct atmospheric deposition (Foucher and Hintelmann, 2009; Gehrke et al., 2009; Yin et al., 2015). In contrast to these steady state conditions, extinction events and OAEs are often associated with rapid increase in the overall input of Hg (and almost all other natural materials) to the atmospheric-ocean-terrestrial system, with simultaneous environmental perturbations such as wildfires, increased soil erosion, and enhanced loading of aerosols, which can potentially be revealed by Hg isotope signals. In recent work, Hg isotopes (especially MIF of ^{199}Hg and ^{201}Hg) have provided critical insights into the sources of Hg in the geologic past (Gong et al., 2017; Grasby et al., 2017; Huang et al., 2018; Sial et al., 2016; Them et al., 2019; Thibodeau et al., 2016; Wang et al., 2018).

We examined all published Hg isotope data from extinction studies to-date to provide an overview of the range of values, with a focus on the two more important systems: Δ^{199}Hg and δ^{202}Hg. These data are plotted in Fig. 13 and show mean (and range) of values of Δ^{199}Hg = 0.052‰ (−0.3 to 0.27‰) and δ^{202}Hg = −1.07‰ (−2.3–0.23‰). The range of Hg isotope values reported for extinction studies are thus similar to the range of values reported by Blum et al. (2014) for rocks and pre-anthropogenic marine sediments, indicating that the range of Hg sources to the environment (atmosphere/terrestrial/volcanic) and their associated fractionations may have been consistent through geologic time.

Sial et al. (2016) examined Hg enrichments across several KPg boundary sections and observed positive Δ^{199}Hg associated with Hg enrichments, arguing for direct atmospheric deposition to the marine environment of Hg^{2+} − attributed to the Deccan Traps. In a similar study, Thibodeau et al. (2016) observed Hg enrichments across the Triassic/Jurassic boundary from Muller Canyon, Nevada (USA) and argue that Δ^{199}Hg and Δ^{201}Hg values are consistent with atmospheric loading, which they attributed to eruption of the Central Atlantic Magmatic Province. Gong et al. (2017) also recognised positive Δ^{199}Hg values associated with the Hg spike at the Ordovician-Silurian mass extinction from marine section in the Yichang area of South China (attributed to an uncertain LIP event).

A similar stable isotope signature was observed for Hg enrichments across the Latest Permian extinction from deep water records at Buchanan Lake, Arctic Canada, with small positive Δ^{199}Hg values (Grasby et al., 2017) attributed to volcanic loading from the Siberian Traps. Grasby et al. (2017) also demonstrate, however, that a shallow

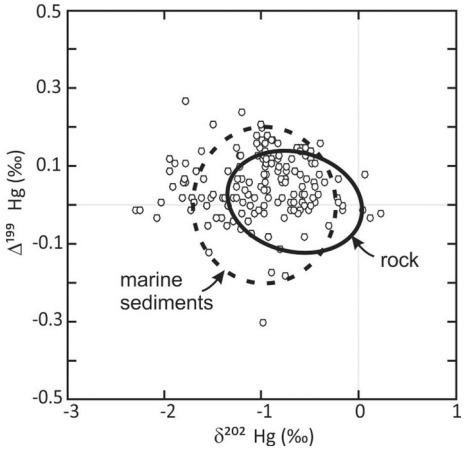

Fig. 13. Plot of stable isotope values of mercury from reported data (dots) along with the 67% data range ellipsoids of Blum et al. (2014) for pre-anthropogenic marine sediments and rocks.

marine record across the LPE (Meishan section, South China) that also has Hg enrichments shows a sharp decrease in Δ^{199}Hg values. They suggest that in this case the shallow water setting records an Hg enrichment related to terrestrial sources driven by massive wildfires (as evidenced by high PAH values) and enhanced soil erosion. This study provided critical new insight that not all Hg anomalies can be directly attributed to enhanced volcanic input, and terrestrial disruption could also be a source of high Hg in the marine record. A similar stable isotope study demonstrated atmospheric-sourced Hg as the dominant cause of Hg spikes in deep-water records across the LPE (Daxiakou and Shangsi sections of South China), in contrast to terrestrially sourced Hg in shallow water sections (Wang et al., 2018).

Them et al. (2019) demonstrated for the Toarcian Oceanic Anoxic Event that 1) Hg spikes are limited to nearshore environments and not present in deeper marine records, 2) there are stratigraphic enrichments suggesting temporal offsets in Hg loading to particular sites, and 3) local redox played a significant role in Hg sequestration. The Hg stable isotope data from this study also suggest that these nearshore Hg spikes most likely had a terrestrial source. These results draw into question the conclusion of Percival et al. (2015) that Toarcian Hg spikes are directly linked to volcanogenic outgassing of Hg from the Karoo–Ferrar Large Igneous Province. It could be argued, however, that the terrestrially derived Hg spike was caused by landscape devastation related to volcanism (Them et al., 2017), and thus still an indirect linkage (Them et al., 2019). Regardless, there is a bias toward the preservation of sedimentary successions in epicontinental, epeiric, and marginal marine environments, so Hg enrichments from these locations require multiple geochemical datasets to confidently link their accumulation directly to LIPs.

Mercury stable isotopes have also been employed to address the ongoing controversy of the relative impact of the Deccan Trap eruptions versus bolide impact for the KPg extinction (as discussed in Burgess, 2019). Here, Sial et al. (2016, 2019) have examined Hg stable isotopes from several sections that suggest the Hg spike at the KPg extinction boundary is largely volcanically sourced. These authors caution, however, that these results are not definitive and more research on Hg isotope systematics are required.

A compilation of all Hg stable isotope data to-date compared to reported Hg concentrations provides some interesting trends as observed in Fig. 14. There are two significant trends associated with Δ^{199}Hg and Δ^{201}Hg values and Hg contents; one is a slight positive shift and the other is more sharply negative. Consistent with previous interpretations (Grasby et al., 2017), these trends suggest the largest observed Hg spikes may be volcanically sourced (whether proximal or distal to the study location), and the slight positive shift could reflect Hg^{2+} absorbed from the atmosphere by volcanic plume particles, rather than direct atmospheric deposition. A lesser Hg spike associated with a negative Δ^{199}Hg signature can be related to terrestrial Hg sources. These results support a general model of how Hg spikes can be formed in response to a LIP eruption. The LIP eruption itself can greatly increase the direct Hg flux to the atmosphere, which is then diffused by global circulation and transport, and deposited in dominantly in ocean basins.

To-date, data suggest that Hg signatures related to LIPs may be best recorded in deep marine sections, but not all LIP events have such an associated Hg record from these environments. This may reflect cases where the there is either insufficient net increase in Hg loading rates to the atmosphere or conditions to drawdown excess Hg loading to marine systems are not sufficient to record an Hg spike (e.g., as suggested for the Toarcian). In contrast, devastation of terrestrial environments by LIP events can release a lower overall mass of Hg (see above). In this case, Hg is transported through riverine systems and as such more limited in its dispersal to the marine environment to nearshore areas. Although estimates of these terrestrial fluxes are less significant than Hg released from a LIP event, they are more localised and concentrated. For instance, Them et al. (2019) estimated landscape disturbance through the Toarcian OAE cycled an additional 330 Mt. Hg to the environment over ~300 ky. This can locally overwhelm any atmospheric signature, as shown for the LPE (Grasby et al., 2017; Wang et al., 2018), or be the only signature as for the Toarcian (Them et al., 2019).

8. Conclusions

Over the last decade there has been significant interest is examining Hg chemostratigraphy at times of major environmental crises throughout the Phanerozoic. Numerous researchers have suggested Hg anomalies directly link LIP events as the ultimate driver of these crises. The body of this work clearly demonstrates that Hg anomalies are a common feature in sedimentary records at times of mass extinction and ocean anoxic events, which are also contemporaneous with widespread environmental disturbances. It is clear that these Hg spikes are not always a definitive signature in themselves of enhanced volcanic emissions. As more data are generated in the future, there may be more confidence in assigning a volcanic driver to Hg spikes, as there are several strong cases already, and conceptually an Hg anomaly would be expected during LIPs. Yet there is much complexity in the global Hg cycle that needs to be resolved in the modern to fully understand what an Hg spike reflects in the sedimentary record. Care is required to fully examine all potential pathways for Hg sequestration, which includes drawdown by OM and sulphide minerals as well as sorption onto clay minerals and Fe oxides, before definitive links to volcanism can be made. Certain basics standards are also required for future work that includes use of appropriate analytical methods and using care not to interpret data below detection limits of analytical equipment (as occurs far too often). Incorporation of Hg stable isotopes to better resolve sources and pathways will also help elucidate the true nature of observed Hg anomalies.

The tremendous volume of data produced over the last several years does provide much greater insight into Hg in the geologic record. We propose a new average value for Hg in clastic sedimentary rocks of 62.4 μg/kg, a lower value for limestone of 34.3 μg/kg, as well an average value of Hg/TOC in sediments of 71.9 μg/kg/wt%. If such values are used as reference to what constitutes an “anomaly,” then several studies fail to pass this bar and perhaps should be reassessed. Studies based on TOC values below analytical certainty (0.2 wt%) should be questioned. Furthermore, the local depositional environment must be characterized as locally reducing water column or sediments may result in values higher than these averages. We also demonstrate that the range of values of Hg isotopes, both MDF and MIF in the rock record are similar to pre-anthropogenic sediments, indicating that the processes controlling the global Hg cycle have likely been relatively consistent through the Phanerozoic, and may make good signatures.

The underlying enthusiasm for use of Hg as a proxy for volcanism is that its release during an eruption should be widespread and recorded in sediments. Mercury is but one volcanogenic metal with potential to be released by LIP events (Grasby et al., 2015). The authors in that study estimated rates of metal loading rates by the Siberian Trap eruptions that ranged from 107% to 977% for Se and Co, respectively. The list of metals with enhanced loading rates also include: As, Cd, Co, Cr, Cu, Hg, Mn, Mo, Ni, Pb, Sb, Se, V, and Zn. Thus, other metals should also be assessed in sedimentary records as a mark left by massive volcanic eruptions, but widespread reducing conditions and changes in the global redox state of the oceans (e.g. Ostrander et al., 2017; Them et al., 2018) may make this difficult as many of these elements are also sensitive to the reduction-oxidation (redox) potential of the oceans. We suggest these geochemical proxies be collectively be reference to as “LIP marks”. Collectively, these can provide further understanding of the potential role of LIP events as a major driver of environmental crisis throughout Earth history.

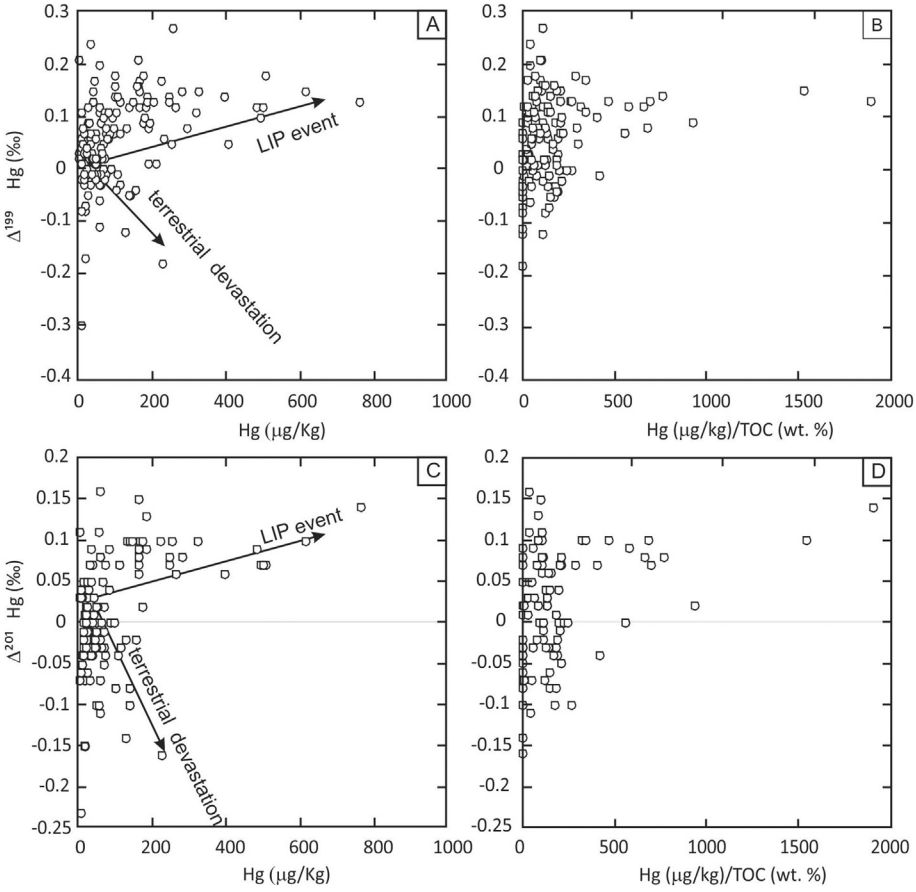

Fig. 14. Plot of published Hg stable isotope data to date relative to reported Hg concentrations and the Hg/TOC ratio. Plots show: (A) Δ199Hg versus Hg concentration, and (B) the Hg/TOC ratio. Similarly, (C) Δ201Hg is plotted against Hg concentration, and (D) the Hg/TOC ratio.

Acknowledgements

We appreciate comments from three reviewers that helped improve the manuscript.

References

AMAP, 2011. AMAP Assessment 2011: Mercury in the Arctic. Arctic Monitoring and Assessment Programme (AMAP), Oslo, Norway.
Amos, H.M., Jacob, D.J., Kocman, D., Horowitz, H.M., Zhang, Y., Dutkiewicz, S., Horvat, M., Corbitt, E.S., Krabbenhoft, D.P., Sunderland, E.M., 2014. Global biogeochemical implications of mercury discharges from rivers and sediment burial. Environ. Sci. Technol. 48 (16), 9514–9522.
Ansmann, A., Mattis, I., Wandinger, U., Wagner, F., Reichardt, J., Deshler, T., 1997. Evolution of the Pinatubo aerosol: Raman lidar observations of particle optical depth, effective radius, mass, and surface area over Central Europe at 53.4°N. J. Atmos. Sci. 54 (22), 2630–2641.
Aston, F.W., 1925. The isotopes of mercury. Nature 116, 208.
Bagnato, E., Aiuppa, A., Parello, F., Calabrese, S., D'Alessandro, W., Mather, T.A., McGonigle, A.J.S., Pyle, D.M., Wängberg, I., 2007. Degassing of gaseous (elemental and reactive) and particulate mercury from Mount Etna volcano (Southern Italy). Atmos. Environ. 41 (35), 7377–7388.
Bagnato, E., Oliveri, E., Acquavita, A., Covelli, S., Petranich, E., Barra, M., Italiano, F., Parello, F., Sprovieri, M., 2017. Hydrochemical mercury distribution and air-sea exchange over the submarine hydrothermal vents off-shore Panarea Island (Aeolian arc, Tyrrhenian Sea). Mar. Chem. 194, 63–78.
Behar, F., Beaumont, V., De B. Penteado, H.L., 2001. Rock-Eval 6 technology: performances and developments. Oil Gas Sci. Technol. 56 (2), 111–134.
Benoit, J.M., Mason, R.P., Gilmour, C.C., Aiken, G.R., 2001. Constants for mercury binding by dissolved organic matter isolates from the Florida Everglades. Geochim. Cosmochim. Acta 65 (24), 4445–4451.
Bergquist, B.A., Blum, J.D., 2007. Mass-dependent and -independent fractionation of Hg Isotopes by photoreduction in aquatic systems. Science 318 (5849), 417–420.
Bergquist, B.A., Blum, J.D., 2009. The odds and evens of mercury isotopes: applications of mass-dependent and mass-independent isotope fractionation. Elements 5, 353–357.
Biswas, A., Blum, J.D., Bergquist, B.A., Keeler, G.J., Xie, Z., 2008. Natural mercury isotope variation in coal deposits and organic soils. Environ. Sci. Technol. 42 (22), 8303–8309.
Bisutti, I., Hilke, I., Raessler, M., 2004. Determination of total organic carbon–an overview of current methods. TrAC Trends in Analytical Chemistry 23 (10-11), 716–726.
Blum, J.D., Bergquist, B.A., 2007. Reporting of variations in the natural isotopic composition of mercury. Anal. Bioanal. Chem. 388 (2), 353–359.
Blum, J.D., Johnson, M.W., 2017. Recent developments in mercury stable isotope analysis. Rev. Mineral. Geochem. 82 (1), 733–757.
Blum, J.D., Sherman, L.S., Johnson, M.W., 2014. Mercury isotopes in earth and environmental sciences. Annu. Rev. Earth Planet. Sci. 42 (1), 249–269.
Bluth, G.J.S., Doiron, S.D., Schnetzler, C.C., Krueger, A.J., Walter, L.S., 1992. Global tracking of the SO2 clouds from the June, 1991 Mount Pinatubo eruptions. Geophys. Res. Lett. 19 (2), 151–154.
Bond, D.P.G., Grasby, S.E., 2017. On the causes of mass extinctions. Palaeogeogr. Palaeoclimatol. Palaeoecol. 478, 3–29.
Bond, D.P.G., Wignall, P.B., 2014. Large igneous provinces and mass extinctions: an update. In: Keller, G., Kerr, A.C. (Eds.), Volcanism, Impacts, and Mass Extinctions: Causes and Effects. The Geological Society of America.
Bower, J., Savage, K.S., Weinman, B., Barnett, M.O., Hamilton, W.P., Harper, W.F., 2008. Immobilization of mercury by pyrite (FeS2). Environ. Pollut. 156 (2), 504–514.
Bowman, K.L., Hammerschmidt, C.R., Lamborg, C.H., Swarr, G., 2015. Mercury in the North Atlantic Ocean: the U.S. GEOTRACES zonal and meridional sections. Deep-Sea Res. II Top. Stud. Oceanogr. 116, 251–261.
Burgess, S., 2019. Deciphering mass extinction triggers. 363 (6429), 815–816.
Carvajal-Ortiz, H., Gentzis, T., 2015. Critical considerations when assessing hydrocarbon plays using Rock-Eval pyrolysis and organic petrology data: data quality revisited. Int. J. Coal Geol. 152, 113–122.
Charbonnier, G., Föllmi, K.B., 2017. Mercury enrichments in lower Aptian sediments support the link between Ontong Java large igneous province activity and oceanic anoxic episode 1a. Geology 45 (1), 63–66.
Charbonnier, G., Morales, C., Duchamp-Alphonse, S., Westermann, S., Adatte, T., Föllmi, K.B., 2017. Mercury enrichment indicates volcanic triggering of Valanginian environmental change. Sci. Rep. 7, 40808.
Chen, J., Hintelmann, H., Feng, X., Dimock, B., 2012. Unusual fractionation of both odd and even mercury isotopes in precipitation from Peterborough, ON, Canada. Geochim. Cosmochim. Acta 90, 33–46.
Courtillot, V.E., Renne, P.R., 2003. On the ages of flood basalt events. Compt. Rendus Geosci. 335 (1), 113–140.
Courtillot, V., Jaupart, C., Manighetti, I., Tapponnier, P., Besse, J., 1999. On causal links between flood basalts and continental breakup. Earth Planet. Sci. Lett. 166 (3–4),

177–195.
de Lacerda, L.D., Turcq, B., Sifeddine, A., Cordeiro, R.C., 2017. Mercury accumulation rates in Caço Lake, NE Brazil during the past 20.000 years. J. S. Am. Earth Sci. 77, 42–50.
Dean, W.E., 1974. Determination of carbonate and organic matter in calcareous sediments and sedimentary rocks by loss on ignition; comparison with other methods. J. Sediment. Res. 44 (1), 242–248.
Demers, J.D., Blum, J.D., Zak, D.R., 2013. Mercury isotopes in a forested ecosystem: implications for air-surface exchange dynamics and the global mercury cycle. Glob. Biogeochem. Cycles 27 (1), 222–238.
Driscoll, C.T., Mason, R.P., Chan, H.M., Jacob, D.J., Pirrone, N., 2013. Mercury as a global pollutant: sources, pathways, and effects. Environ. Sci. Technol. 47 (10), 4967–4983.
Enrico, M., Roux, G.L., Marusczak, N., Heimbürger, L.-E., Claustres, A., Fu, X., Sun, R., Sonke, J.E., 2016. Atmospheric mercury transfer to peat bogs dominated by gaseous elemental mercury dry deposition. Environ. Sci. Technol. 50 (5), 2405–2412.
Ericksen, J.A., Gustin, M.S., Schorran, D.E., Johnson, D.W., Lindberg, S.E., Coleman, J.S., 2003. Accumulation of atmospheric mercury in forest foliage. Atmos. Environ. 37 (12), 1613–1622.
Ernst, R.E., Youbi, N., 2017. How large Igneous Provinces affect global climate, sometimes cause mass extinctions, and represent natural markers in the geological record. Palaeogeogr. Palaeoclimatol. Palaeoecol. 478, 30–52.
Fantasia, A., Föllmi, K.B., Adatte, T., Bernárdez, E., Spangenberg, J.E., Mattioli, E., 2018. The Toarcian oceanic anoxic event in southwestern gondwana: an example from the Andean Basin, northern Chile. J. Geol. Soc. 175, 883–902 (jgs2018-008).
Feyte, S., Gobeil, C., Tessier, A., Cossa, D., 2012. Mercury dynamics in lake sediments. Geochim. Cosmochim. Acta 82, 92–112.
Fitzgerald, W.F., Lamborg, C.H., 2014. Geochemistry of mercury in the environment. Treatise Geochem. 11.
Fleck, J.A., Grigal, D.F., Nater, E.A., 1999. Mercury uptake by trees: an observational experiment. Water Air Soil Pollut. 115 (1), 513–523.
Fleischer, M., 1970. Summary of the Literature on the Inorganic Geochemnistry of Mercury, Mercury in the Environment. USGS Professional Paper 713. USGS, Washington, DC.
Font, E., Adatte, T., Sial, A.N., Drude de Lacerda, L., Keller, G., Punekar, J., 2016. Mercury anomaly, Deccan volcanism, and the end-Cretaceous mass extinction. Geology 44 (2), 171–174.
Foucher, D., Hintelmann, H., 2006. High-precision measurement of mercury isotope ratios in sediments using cold-vapor generation multi-collector inductively coupled plasma mass spectrometry. Anal. Bioanal. Chem. 384 (7), 1470–1478.
Foucher, D., Hintelmann, H., 2009. Tracing mercury contamination from the Idrija Mining Region (Slovenia) to the gulf of trieste using Hg isotope ratio measurements. Environ. Sci. Technol. 43 (1), 33–39.
Frescholtz, T.F., Gustin, M.S., Schorran, D.E., Fernandez, G.C.J., 2003. Assessing the source of mercury in foliar tissue of quaking aspen. Environ. Toxicol. Chem. 22 (9), 2114–2119.
Gehrke, G.E., Blum, J.D., Meyers, P.A., 2009. The geochemical behavior and isotopic composition of Hg in a mid-Pleistocene western Mediterranean sapropel. Geochim. Cosmochim. Acta 73 (6), 1651–1665.
Gelety, V.F., Kalmykov, G.V., Parkhomenko, I.Y., 2007. Mercury in the sedimentary deposits of Lake Baikal. Geochem. Int. 45 (2), 170–177.
Gleckler, P.J., Wigley, T.M.L., Santer, B.D., Gregory, J.M., AchutaRao, K., Taylor, K.E., 2006. Krakatoa's signature persists in the ocean. Nature 439 (7077), 675.
Global Volcanism Program, 2013. In: Venzke, E. (Ed.), Volcanoes of the World. Smithsonian Institution.
Gobeil, C., Cossa, D., 1993. Mercury in sediments and sediment pore water in the Laurentian Trough. Can. J. Fish. Aquat. Sci. 50 (8), 1794–1800.
Gobeil, C., Macdonald, R.W., Smith, J.N., 1999. Mercury profiles in sediments of the Arctic Ocean Basins. Environ. Sci. Technol. 33 (23), 4194–4198.
Gong, Q., Wang, X., Zhao, L., Grasby, S.E., Chen, Z.-Q., Zhang, L., Li, Y., Cao, L., Li, Z., 2017. Mercury spikes suggest volcanic driver of the Ordovician-Silurian mass extinction. Sci. Rep. 7 (1), 5304.
Goodsite, M.E., Outridge, P.M., Christensen, J.H., Dastoor, A., Muir, D., Travnikov, O., Wilson, S., 2013. How well do environmental archives of atmospheric mercury deposition in the Arctic reproduce rates and trends depicted by atmospheric models and measurements? Sci. Total Environ. 452-453, 196–207.
Grasby, S.E., Sanei, H., Beauchamp, B., 2011. Catastrophic dispersion of coal fly ash into oceans during the latest Permian extinction. Nat. Geosci. 4 (2), 104–107.
Grasby, S.E., Beauchamp, B., Embry, A.F., Sanei, H., 2013a. Recurrent early Triassic ocean anoxia. Geology 41, 175–178.
Grasby, S.E., Sanei, H., Beauchamp, B., Chen, Z., 2013b. Mercury deposition through the Permo–Triassic Biotic Crisis. Chem. Geol. 351, 209–216.
Grasby, S.E., Beauchamp, B., Bond, D.P.G., Wignall, P.B., Talavera, C., Galloway, J.M., Piepjohn, K., Reinhardt, L., Blomeier, D., 2015. Progressive environmental deterioration in NW Pangea leading to the latest Permian extinction. Geol. Soc. Am. Bull. 127 (9/10), 1331–1347.
Grasby, S.E., Beauchamp, B., Bond, D.P.G., Wignall, P.B., Sanei, H., 2016. Mercury anomalies associated with three extinction events (Capitanian Crisis, latest Permian Extinction and the Smithian/Spathian Extinction) in NW Pangea. Geol. Mag. 153 (2), 285–297.
Grasby, S.E., Shen, W., Yin, R., Gleason, J.D., Blum, J.D., Lepak, R.F., Hurley, J.P., Beauchamp, Benoit, 2017. Isotopic signatures of mercury contamination in latest Permian oceans. Geology 45 (1), 55–58.
Gratz, L.E., Keeler, G.J., Blum, J.D., Sherman, L.S., 2010. Isotopic composition and fractionation of mercury in Great Lakes precipitation and ambient air. Environ. Sci. Technol. 44 (20), 7764–7770.
Gröcke, D.R., Rimmer, S.M., Yoksoulian, L.E., Cairncross, B., Tsikos, H., van Hunen, J., 2009. No evidence for thermogenic methane release in coal from the Karoo-Ferrar large igneous province. Earth Planet. Sci. Lett. 277 (1), 204–212.
Han, D.S., Orillano, M., Khodary, A., Duan, Y., Batchelor, B., Abdel-Wahab, A., 2014. Reactive iron sulfide (FeS)-supported ultrafiltration for removal of mercury (Hg(II)) from water. Water Res. 53, 310–321.
Heiri, O., Lotter, A.F., Lemcke, G., 2001. Loss on ignition as a method for estimating organic and carbonate content in sediments: reproducibility and comparability of results. J. Paleolimnol. 25 (1), 101–110.
Hildebrand, A.R., Boynton, W.V., 1989. Hg anomalies at the K/T boundary: evidence for acid rain? In: 52nd Annual Meeting of the Meteoritical Society. Lunar and Planetary Institute, Vienna, Austria, pp. 89.
Hinkley, T.K., Lamothe, P.J., Wilson, S.A., Finnegan, D.L., Gerlach, T.M., 1999. Metal emissions from Kilauea, and a suggested revision of the estimated worldwide metal output by quiescent degassing of volcanoes. Earth Planet. Sci. Lett. 170 (3), 315–325.
Holmes, C.D., Jacob, D.J., Corbitt, E.S., Mao, J., Yang, X., Talbot, R., Slemr, F., 2010. Global atmospheric model for mercury including oxidation by bromine atoms. Atmos. Chem. Phys. 10, 12037–12057.
Huang, Y., Chen, Z.-Q., Wignall, P.B., Grasby, S.E., Zhao, L., Wang, X., Kaiho, K., 2018. Biotic responses to volatile volcanism and environmental stresses over the Guadalupian-Lopingian (Permian) transition. Geology 47 (2), 175–178.
Jarvie, D.M., 1991. Total organic carbon (TOC) analysis. In: Merrill, R.K. (Ed.), Treatise of Petroleum Geology: Handbook of Petroleum Geology, Source and Migration Processes and Evaluation Techniques. American Association of Petroleum Geologists, pp. 113–118.
Jones, D.S., Martini, A.M., Fike, D.A., Kaiho, K., 2017. A volcanic trigger for the late Ordovician mass extinction? Mercury data from South China and Laurentia. Geology 45 (7), 631–634.
Jones, M.T., Percival, L.M.E., Stokke, E.W., Frieling, J., Mather, T.A., Riber, L., Schubert, B.A., Schultz, B., Tegner, C., Planke, S., Svensen, H.H., 2019. Mercury anomalies across the Palaeocene–Eocene thermal maximum. Clim. Past 15 (1), 217–236.
Keller, G., Mateo, P., Punekar, J., Khozyem, H., Gertsch, B., Spangenberg, J., Bitchong, A.M., Adatte, T., 2018. Environmental changes during the cretaceous-Paleogene mass extinction and Paleocene-Eocene thermal maximum: implications for the anthropocene. Gondwana Res. 56, 69–89.
Kim, C.S., Rytuba, J.J., Brown, G.E., 2004. EXAFS study of mercury(II) sorption to Fe- and Al-(hydr)oxides: I. Effects of pH. J. Colloid Interface Sci. 271 (1), 1–15.
Krupp, R., 1988. Physicochemical aspects of mercury metallogenesis. Chem. Geol. 69 (3), 345–356.
Kumar, A., Wu, S., Huang, Y., Liao, H., Kaplan, J.O., 2018. Mercury from wildfires: Global emission inventories and sensitivity to 2000–2050 global change. Atmos. Environ. 173, 6–15.
Lafargue, E., Espitalité, J., Marquis, F., Pillot, D., 1998. Rock-Eval 6 applications in hydrocarbon exploration, production and soil contamination studies. Rev. Inst. Fr. Pet. 53 (4), 421–437.
Lamborg, C.H., Von Damm, K.L., Fitzgerald, W.F., Hammerschmidt, C.R., Zierenberg, R., 2006. Mercury and monomethylmercury in fluids from Sea Cliff submarine hydrothermal field, Gorda Ridge. Geophys. Res. Lett. 33 (17).
Lamborg, C.H., Hammerschmidt, C.R., Bowman, K.L., 2016. An examination of the role of particles in oceanic mercury cycling. Phil. Trans. A Math. Phys. Eng. Sci. 374 (2081), 20150297.
Lauretta, D.S., Klaue, B., Blum, J.D., Buseck, P.R., 2001. Mercury abundances and isotopic compositions in the Murchison (CM) and Allende (CV) carbonaceous chondrites. Geochim. Cosmochim. Acta 65 (16), 2807–2818.
Lin, C.-J., Pehkonen, S.O., 1999. The chemistry of atmospheric mercury: a review. Atmos. Environ. 33 (13), 2067–2079.
Lindberg, S.E., Andrenson, A.W., Harrisson, R.C., 1975. Geochemistry of mercury in the estuarine environment. In: Cronin, E.L. (Ed.), Estuarine Research. Chemistry, Biology and the Estuarine System. Cronin. Academic Press, New York.
Liu, M., Chen, D., Zhou, X., Yuan, W., Jiang, M., Liu, L., 2019. Climatic and oceanic changes during the Middle-late Ordovician transition in the Tarim Basin, NW China and implications for the Great Ordovician Biodiversification Event. Palaeogeogr. Palaeoclimatol. Palaeoecol. 514, 522–535.
Lockhart, W.L., Macdonald, R.W., Outridge, P.M., Wilkinson, P., DeLaronde, J.B., Rudd, J.W.M., 2000. Tests of the fidelity of lake sediment core records of mercury deposition to known histories of mercury contamination. Sci. Total Environ. 260 (1), 171–180.
Majorowicz, J., Osadetz, K., Safanda, J., 2012a. Gas hydrate formation and dissipation histories in the northern margin of Canada: beaufort-mackenzie and the Sverdrup basins. J. Geol. Res. 17.
Majorowicz, J., Safanda, J., Osadetz, K., 2012b. Inferred gas hydrate and permafrost stability history models linked to climate change in the Beaufort-Mackenzie Basin, Arctic Canada. Clim. Past 8 (2), 667–682.
Majorowicz, J., Grasby, S.E., Safanda, J., Beauchamp, B., 2014. Gas hydrate contribution to late Permian global warming. Earth Planet. Sci. Lett. 393, 243–253.
Mangold, J.E., Park, C.M., Liljestrand, H.M., Katz, L.E., 2014. Surface complexation modeling of Hg(II) adsorption at the goethite/water interface using the charge distribution Multi-Site Complexation (CD-MUSIC) model. J. Colloid Interface Sci. 418, 147–161.
Nascimento-Silva, M.V., Sial, A.N., Ferreira, V.P., Neumann, V.H., Barbosa, J.A., Pimentel, M.M., de Lacerda, L.D., 2011. Cretaceous-Paleogene transition at the Paraíba Basin, Northeastern, Brazil: Carbon-isotope and mercury subsurface stratigraphies. J. S. Am. Earth Sci. 32 (4), 379–392.
Nriagu, J., Becker, C., 2003. Volcanic emissions of mercury to the atmosphere: global and regional inventories. Sci. Total Environ. 304 (1–3), 3–12.
Obrist, D., Agnan, Y., Jiskra, M., Olson, C.L., Colegrove, D.P., Hueber, J., Moore, C.W., Sonke, J.E., Helmig, D., 2017. Tundra uptake of atmospheric elemental mercury

drives Arctic mercury pollution. Nature 547, 201.
Ogden, D.E., Sleep, N.H., 2012. Explosive eruption of coal and basalt and the end-Permian mass extinction. Proc. Natl. Acad. Sci. 109 (1), 59–62.
Ostrander, C.M., Owens, J.D., Nielsen, S.G., 2017. Constraining the rate of oceanic deoxygenation leading up to a cretaceous Oceanic Anoxic Event (OAE-2: ~94 Ma). 3 (8), e1701020.
Outridge, P.M., Wang, F., 2015. The stability of metal profiles in freshwater and marine sediments. In: Blais, J.M., Rosen, M.R., Smol, J.P. (Eds.), Environmental Contaminants: Using Natural Archives to Track Sources and Long-Term Trends of Pollution. Springer Netherlands, Dordrecht, pp. 35–60.
Outridge, P.M., Sanei, H., Stern, G.A., Hamilton, P.B., Goodarzi, F., 2007. Evidence for control of mercury accumulation in sediments by variations of aquatic primary productivity in Canadian High Arctic lakes. Environ. Sci. Technol. 41, 5259–5265.
Palinkaš, L., Drobne, K., Durn, G., Miko, S., 1996. Mercury anomaly at the cretaceous -Tertiary boundry; Dolenja Vas, Slovenia. In: Drobne, K., Goričan, Š., Kotnik, B. (Eds.), International Workshop POSTOJNA 96: The Role of Impact Processes in the Geological and Biological Evolution of the Planet Earth, Postojna, Slovenija, pp. 57–60.
Paschall, O., Carmichael, S.K., Königshof, P., Waters, J.A., Ta, P.H., Komatsu, T., Dombrowski, A., 2019. The Devonian-Carboniferous boundary in Vietnam: sustained ocean anoxia with a volcanic trigger for the Hangenberg Crisis? Glob. Planet. Chang. 175, 64–81.
Percival, J.B., Outridge, P.M., 2013. A test of the stability of Cd, Cu, Hg, Pb and Zn profiles over two decades in lake sediments near the Flin Flon Smelter, Manitoba, Canada. Sci. Total Environ. 454-455, 307–318.
Percival, L.M.E., Witt, M.L.I., Mather, T.A., Hermoso, M., Jenkyns, H.C., Hesselbo, S.P., Al-Suwaidi, A.H., Storm, M.S., Xu, W., Ruhl, M., 2015. Globally enhanced mercury deposition during the end-Pliensbachian extinction and Toarcian OAE: a link to the Karoo–Ferrar large Igneous Province. Earth Planet. Sci. Lett. 428, 267–280.
Percival, L.M.E., Ruhl, M., Hesselbo, S.P., Jenkyns, H.C., Mather, T.A., Whiteside, J.H., 2017. Mercury evidence for pulsed volcanism during the end-Triassic mass extinction. Proc. Natl. Acad. Sci. 114 (30), 7929–7934.
Percival, L.M.E., Jenkyns, H.C., Mather, T.A., Dickson, A.J., Batenburg, S.J., Ruhl, M., Hesselbo, S.P., Barclay, R., Jarvis, I., Robinson, S.A., Woelders, L., 2018. Does large igneous province volcanism always perturb the mercury cycle? Comparing the records of Oceanic Anoxic event 2 and the end-cretaceous to other Mesozoic events. 318 (8), 799–860.
Pirrone, N., Cinnirella, S., Feng, X., Finkelman, R.B., Friedli, H.R., Leaner, J., Mason, R., Mukherjee, A.B., Stracher, G.B., Streets, D.G., Telmer, K., 2010. Global mercury emissions to the atmosphere from anthropogenic and natural sources. Atmos. Chem. Phys. Discuss. 10, 4719–4752.
Pruss, S.B., Jones, D.S., Fike, D.A., Tosca, N.J., Wignall, P.B., 2019. Marine anoxia and sedimentary mercury enrichments during the late Cambrian SPICE event in northern Scotland. Geology 47 (5), 475–478.
Pyle, D.M., Mather, T.A., 2003. The importance of volcanic emissions for the global atmospheric mercury cycle. Atmos. Environ. 37 (36), 5115–5124.
Racki, G., Rakociński, M., Marynowski, L., Wignall, P.B., 2018. Mercury enrichments and the Frasnian–Famennian biotic crisis: a volcanic trigger proved? Geology 46 (6), 543–546.
Raven, M.R., Adkins, J.F., Werne, J.P., Lyons, T.W., Sessions, A.L., 2015. Sulfur isotopic composition of individual organic compounds from Cariaco Basin sediments. Org. Geochem. 80, 53–59.
Raven, M.R., Fike, D.A., Gomes, M.L., Webb, S.M., Bradley, A.S., McClelland, H.-L.O., 2018. Organic carbon burial during OAE2 driven by changes in the locus of organic matter sulfurization. Nat. Commun. 9 (1), 3409.
Ravichandran, M., 2004. Interactions between mercury and dissolved organic matter – a review. Chemosphere 55 (3), 319–331.
Reichow, M.K., Pringle, M.S., Al'Mukhamedov, A.I., Allen, M.B., Andreichev, V.L., Buslov, M.M., Davies, C.E., Fedoseev, G.S., Fitton, J.G., Inger, S., Medvedev, A.Y., Mitchell, C., Puchkov, V.N., Safonova, I.Y., Scott, R.A., Saunders, A.D., 2009. The timing and extent of the eruption of the Siberian Traps large igneous province: implications for the end-Permian environmental crisis. Earth Planet. Sci. Lett. 277, 9–20.
Ribeiro Guevara, S., Meili, M., Rizzo, A., Daga, R., Arribére, M., 2010. Sediment records of highly variable mercury inputs to mountain lakes in Patagonia during the past millennium. Atmos. Chem. Phys. 10, 3443–3453.
Robock, A., 2000. Volcanic eruptions and climate. Rev. Geophys. 38 (2), 191–219.
Robock, A., Matson, M., 1983. Circumglobal transport of the El Chichón volcanic dust cloud. Science 221 (4606), 195–197.
Roos-Barraclough, F., Shotyk, W., 2003. Millennial-scale records of atmospheric mercury deposition obtained from ombrotrophic and minerotrophic peatlands in the Swiss Jura Mountains. Environ. Sci. Technol. 37 (2), 235–244.
Roos-Barraclough, F., Martinez-Cortizas, A., García-Rodeja, E., Shotyk, W., 2002. A 14 500 year record of the accumulation of atmospheric mercury in peat: volcanic signals, anthropogenic influences and a correlation to bromine accumulation. Earth Planet. Sci. Lett. 202 (2), 435–451.
Rudnick, R.L., Gao, S., 2014. 4.1 – composition of the continental crust. In: Holland, H.D., Turekian, K.K. (Eds.), Treatise on Geochemistry, 2nd ed. Elsevier, Oxford, pp. 1–51.
Sabatino, N., Ferraro, S., Coccioni, R., Bonsignore, M., Del Core, M., Tancredi, V., Sprovieri, M., 2018. Mercury anomalies in upper Aptian-lower Albian sediments from the Tethys realm. Palaeogeogr. Palaeoclimatol. Palaeoecol. 495, 163–170.
Sanei, H., Grasby, S.E., Beauchamp, B., 2012. Latest Permian mercury anomalies. Geology 40 (1), 63–66.
Sanei, H., Outridge, P.M., Stern, G.A., Macdonald, R.W., 2014. Classification of mercury–labile organic matter relationships in lake sediments. Chem. Geol. 373, 87–92.
Saunders, A.D., Reichow, M.K., 2009. The Siberian Traps and the End-Permian mass extinction: a critical review. Chin. Sci. Bull. 54, 20–37.
Scaife, J.D., Ruhl, M., Dickson, A.J., Mather, T.A., Jenkyns, H.C., Percival, L.M.E., Hesselbo, S.P., Cartwright, J., Eldrett, J.S., Bergman, S.C., Minisini, D., 2017. Sedimentary mercury enrichments as a marker for submarine large igneous province volcanism? Evidence from the Mid-Cenomanian Event and Oceanic Anoxic Event 2 (Late Cretaceous). Geochem. Geophys. Geosyst. 18 (12), 4253–4275.
Schoene, B., Eddy, M.P., Samperton, K.M., Keller, C.B., Keller, G., Adatte, T., Khadri, S.F.R., 2019. U-Pb constraints on pulsed eruption of the Deccan Traps across the end-Cretaceous mass extinction. Science 363 (6429), 862–866.
Schroeder, W.H., Munthe, J., 1998. Atmospheric mercury—an overview. Atmos. Environ. 32 (5), 809–822.
Schuster, P.F., Krabbenhoft, D.P., Naftz, D.L., Cecil, L.D., Olson, M.L., Dewild, J.F., Susong, D.D., Green, J.R., Abbott, M.L., 2002. Atmospheric mercury deposition during the last 270 years:a glacial ice core record of natural and anthropogenic sources. Environ. Sci. Technol. 36 (11), 2303–2310.
Schuster, P.F., Schaefer, K.M., Aiken, G.R., Antweiler, R.C., Dewild, J.F., Gryziec, J.D., Gusmeroli, A., Hugelius, G., Jafarov, E., Krabbenhoft, D.P., Liu, L., Herman-Mercer, N., Mu, C., Roth, D.A., Schaefer, T., Striegl, R.G., Wickland, K.P., Zhang, T., 2018. Permafrost stores a globally significant amount of mercury. Geophys. Res. Lett. 45 (3), 1463–1471.
Self, S., 2005. The effects and consequences of very large explosive volcanic eruptions. Philos. Trans. R. Soc. Ser. A 364, 2073–2097.
Selin, N.E., 2009. Global biogeochemical cycling of mercury: a review. Annu. Rev. Environ. Resour. 34 (1), 43–63.
Sephton, M.A., Looy, C.V., Brinkhuis, H., Wignall, P.B., de Leeuw, J.W., Visscher, H., 2005. Catastrophic soil erosion during the end-Permian biotic crisis. Geology 33 (12), 941–944.
Shen, W., Sun, Y., Lin, Y., Liu, D., Chai, P., 2011. Evidence for wildfire in the Meishan section and implications for Permian–Triassic events. Geochim. Cosmochim. Acta 75 (7), 1992–2006.
Shen, J., Algeo, T.J., Chen, J., Planavsky, N.J., Feng, Q., Yu, J., Liu, J., 2019. Mercury in marine Ordovician/Silurian boundary sections of South China is sulfide-hosted and non-volcanic in origin. Earth Planet. Sci. Lett. 511, 130–140.
Sherman, L.S., Blum, J.D., Nordstrom, D.K., McCleskey, R.B., Barkay, T., Vetriani, C., 2009. Mercury isotopic composition of hydrothermal systems in the Yellowstone Plateau volcanic field and Guaymas Basin sea-floor rift. Earth Planet. Sci. Lett. 279 (1), 86–96.
Sial, A.N., Gaucher, C., Filho, M.A.d.S., Ferreira, V.P., Pimentel, M.M., Lacerda, L.D., Filho, E.V.S., Cezario, W., 2010. C-, Sr-isotope and Hg chemostratigraphy of Neoproterozoic cap carbonates of the Sergipano Belt, Northeastern Brazil. Precambrian Res. 182 (4), 351–372.
Sial, A.N., Lacerda, L.D., Ferreira, V.P., Frei, R., Marquillas, R.A., Barbosa, J.A., Gaucher, C., Windmöller, C.C., Pereira, N.S., 2013. Mercury as a proxy for volcanic activity during extreme environmental turnover: the Cretaceous–Paleogene transition. Palaeogeogr. Palaeoclimatol. Palaeoecol. 387, 153–164.
Sial, A.N., Chen, J., Lacerda, L.D., Peralta, S., Gaucher, C., Frei, R., Cirilli, S., Ferreira, V.P., Marquillas, R.A., Barbosa, J.A., Pereira, N.S., Belmino, I.K.C., 2014. High-resolution Hg chemostratigraphy: a contribution to the distinction of chemical fingerprints of the Deccan volcanism and Cretaceous–Paleogene Boundary impact event. Palaeogeogr. Palaeoclimatol. Palaeoecol. 414, 98–115.
Sial, A.N., Chen, J., Lacerda, L.D., Frei, R., Tewari, V.C., Pandit, M.K., Gaucher, C., Ferreira, V.P., Cirilli, S., Peralta, S., Korte, C., Barbosa, J.A., Pereira, N.S., 2016. Mercury enrichment and Hg isotopes in Cretaceous–Paleogene boundary successions: Links to volcanism and palaeoenvironmental impacts. Cretac. Res. 66, 60–81.
Sial, A.N., Chen, J., Lacerda, L.D., Frei, R., Higgins, J., Tewari, V.C., Gaucher, C., Ferreira, V.P., Cirilli, S., Peralta, S., Korte, C., Barbosa, J.A., Pereira, N.S., Ramos, D.S., 2019. Chemostratigraphy across the Cretaceous–Paleogene (K/Pg) boundary: testing the impact and volcanism hypotheses. In: Sial, A.N., Gaucher, C., Ramkumar, M., Ferreira, V.P. (Eds.), Chemostratigraphy Across Major Chronological Boundaries. John Wiley & Sons, Inc, pp. 223–257.
Slemr, F., Scheel, H.E., 1998. Trends in atmospheric mercury concentrations at the summit of the Wank mountain, Southern Germany. Atmos. Environ. 32 (5), 845–853.
Sonke, J.E., 2011. A global model of mass independent mercury stable isotope fractionation. Geochim. Cosmochim. Acta 75 (16), 4577–4590.
Sprain, C.J., Renne, P.R., Vanderkluysen, L., Pande, K., Self, S., Mittal, T., 2019. The eruptive tempo of Deccan volcanism in relation to the Cretaceous-Paleogene boundary. 363 (6429), 866–870.
Stern, G.A., Sanei, H., Roach, P., Delaronde, J., Outridge, P.M., 2009. Historical interrelated variations of mercury and aquatic organic matter in lake sediment cores from a subarctic lake in Yukon, Canada: further evidence toward the algal-mercury scavenging hypothesis. Environ. Sci. Technol. 43, 7684–7690.
Štrok, M., Baya, P.A., Hintelmann, H., 2015. The mercury isotope composition of Arctic coastal seawater. Compt. Rendus Geosci. 347 (7), 368–376.
Sun, G., Sommar, J., Feng, X., Lin, C.-J., Ge, M., Wang, W., Yin, R., Fu, X., Shang, L., 2016. Mass-dependent and -independent fractionation of mercury isotope during gas-phase oxidation of elemental mercury vapor by atomic Cl and Br. Environ. Sci. Technol. 50 (17), 9232–9241.
Sun, R., Jiskra, M., Amos, H.M., Zhang, Y., Sunderland, E.M., Sonke, J.E., 2019. Modelling the mercury stable isotope distribution of Earth surface reservoirs: Implications for global Hg cycling. Geochim. Cosmochim. Acta 246, 156–173.
Sunderland, E.M., Mason, R.P., 2007. Human impacts on open ocean mercury concentrations. Glob. Biogeochem. Cycles 21 (4).
Symons, G.J., 1888. The Eruption of Krakatoa, and Subsequent Phenomena. Trubner & co., London, pp. 627.
Them, T.R., Gill, B.C., Selby, D., Gröcke, D.R., Friedman, R.M., Owens, J.D., 2017. Evidence for rapid weathering response to climatic warming during the Toarcian Oceanic Anoxic Event. Sci. Rep. 7 (1), 5003.

Them, T.R., Gill, B.C., Caruthers, A.H., Gerhardt, A.M., Gröcke, D.R., Lyons, T.W., Marroquín, S.M., Nielsen, S.G., Trabucho Alexandre, J.P., Owens, J.D., 2018. Thallium isotopes reveal protracted anoxia during the Toarcian (Early Jurassic) associated with volcanism, carbon burial, and mass extinction. 115 (26), 6596–6601.

Them, T.R., Jagoe, C.H., Caruthers, A.H., Gill, B.C., Grasby, S.E., Gröcke, D.R., Yin, R., Owens, J.D., 2019. Terrestrial sources as the primary delivery mechanism of mercury to the oceans across the Toarcian Oceanic Anoxic Event (Early Jurassic). Earth Planet. Sci. Lett. 507, 62–72.

Thibodeau, A.M., Ritterbush, K., Yager, J.A., West, A.J., Ibarra, Y., Bottjer, D.J., Berelson, W.M., Bergquist, B.A., Corsetti, F.A., 2016. Mercury anomalies and the timing of biotic recovery following the end-Triassic mass extinction. Nat. Commun. 7, 11147.

Thordarson, T., Rampino, M., Keszthelyi, L.P., Self, S., 2009. Effects of megascale eruptions on Earth and Mars. In: Chapman, Mary G., Keszthelyi, Laszlo P. (Eds.), Preservation of Random Megascale Events on Mars and Earth: Influence on Geologic History. vol. 453. Geological Society of America Special Paper, pp. 37–53.

Wang, X., Cawood, P.A., Zhao, H., Zhao, L., Grasby, S.E., Chen, Z.-Q., Wignall, P.B., Lv, Z., Han, C., 2018. Mercury anomalies across the end Permian mass extinction in South China from shallow and deep water depositional environments. Earth Planet. Sci. Lett. 496, 159–167.

Wang, X., Cawood, P.A., Zhao, H., Zhao, L., Grasby, S.E., Chen, Z.-Q., Zhang, L., 2019. Global mercury cycle during the end-Permian mass extinction and subsequent Early Triassic recovery. Earth Planet. Sci. Lett. 513, 144–155.

Wignall, P.B., 2001. Large igneous provinces and mass extinctions. Earth Sci. Rev. 53 (1–2), 1–33.

Witt, M.L.I., Mather, T.A., Pyle, D.M., Aiuppa, A., Bagnato, E., Tsanev, V.I., 2008. Mercury and halogen emissions from Masaya and Telica volcanoes, Nicaragua. J. Geophys. Res. Solid Earth 113 (B6).

Yin, R., Feng, X., Meng, B., 2013. Stable mercury isotope variation in rice plants (*Oryza sativa* L.) from the Wanshan mercury mining district, SW China. Environ. Sci. Technol. 47 (5), 2238–2245.

Yin, R., Feng, X., Li, X., Yu, B., Du, B., 2014. Trends and advances in mercury stable isotopes as a geochemical tracer. Trends Environ. Anal. Chem. 2, 1–10.

Yin, R., Feng, X., Chen, B., Zhang, J., Wang, W., Li, X., 2015. Identifying the sources and processes of mercury in subtropical estuarine and ocean sediments using Hg isotopic composition. Environ. Sci. Technol. 49 (3), 1347–1355.

Yin, R., Feng, X., Hurley, J.P., Krabbenhoft, D.P., Lepak, R.F., Hu, R., Zhang, Q., Li, Z., Bi, X., 2016. Mercury isotopes as proxies to identify sources and environmental impacts of mercury in sphalerites. Sci. Rep. 6, 18686.

Yin, R., Xu, L., Lehmann, B., Lepak, R.F., Hurley, J.P., Mao, J., Feng, X., Hu, R., 2017. Anomalous mercury enrichment in early Cambrian black shales of South China: mercury isotopes indicate a seawater source. Chem. Geol. 467, 159–167.

Yoksoulian, L.E., Rimmer, S.M., Rowe, H.D., 2016. Anatomy of an intruded coal, II: effect of contact metamorphism on organic δ13C and implications for the release of thermogenic methane, Springfield (No. 5) Coal, Illinois Basin. Int. J. Coal Geol. 158, 129–136.

Zaferani, S., Pérez-Rodríguez, M., Biester, H., 2018. Diatom ooze – a large marine mercury sink. Science 361 (6404), 797–800.

Zambardi, T., Sonke, J.E., Toutain, J.P., Sortino, F., Shinohara, H., 2009. Mercury emissions and stable isotopic compositions at Vulcano Island (Italy). Earth Planet. Sci. Lett. 277 (1), 236–243.

Zhang, H., Yin, R.-s., Feng, X.-b., Sommar, J., Anderson, C.W.N., Sapkota, A., Fu, X.-w., Larssen, T., 2013. Atmospheric mercury inputs in montane soils increase with elevation: evidence from mercury isotope signatures. Sci. Rep. 3, 3322.

Zhang, Y., Jacob, D.J., Dutkiewicz, S., Amos, H.M., Long, M.S., Sunderland, E.M., 2015. Biogeochemical drivers of the fate of riverine mercury discharged to the global and Arctic oceans. Glob. Biogeochem. Cycles 29 (6), 854–864.

Zheng, W., Obrist, D., Weis, D., Bergquist, B.A., 2016. Mercury isotope compositions across North American forests. Glob. Biogeochem. Cycles 30 (10), 1475–1492.

Zheng, W., Gilleaudeau, G.J., Kah, L.C., Anbar, A.D., 2018. Mercury isotope signatures record photic zone euxinia in the Mesoproterozoic ocean. Proc. Natl. Acad. Sci. 115 (42), 10594–10599.